Carbohydrate Polymers 247 (2020) 116690

Contents lists available at ScienceDirect

Carbohydrate Polymers

journal homepage: www.elsevier.com/locate/carbpol

Review on recent progress in chitosan/chitin-carbonaceous material composites for the adsorption of water pollutants

M.J. Ahmed[a], B.H. Hameed[b,*], E.H. Hummadi[c]

[a] Department of Chemical Engineering, College of Engineering, University of Baghdad, P.O. Box 47024, Aljadria, Baghdad, Iraq
[b] Department of Chemical Engineering, College of Engineering, Qatar University, P.O. Box 2713, Doha, Qatar
[c] Department of Biotechnology, College of Science, University of Diyala, Baqubah, Iraq

ARTICLE INFO

Keywords:
Biopolymer
Carbonaceous materials
Composite
Water pollutant
Adsorption

ABSTRACT

Chitosan and chitin are categorized as low cost, renewable and eco-friendly biopolymers. However, they have low mechanical properties and unfavorable pore properties in terms of low surface area and total pore volume that limit their adsorption application. Many studies have shown that such weaknesses can be avoided by preparation of composites with carbonaceous materials from these biopolymers. This article provides a systematic review on the preparation of chitosan/chitin-carbonaceous material composites. Commonly used carbonaceous materials such as activated carbon, biochar, carbon nanotubes, graphene oxide and graphene to prepare composites are discussed. The application of chitosan/chitin-carbonaceous material composites for the adsorption of various water pollutants, and the regeneration and reusability of adsorbents are also included. Finally, the challenges and future prospects for the adsorbents applied for the adsorption of water pollutants are summarized.

1. Introduction

Water pollution represents a serious environmental issue that gained great attention mainly due to the development in agricultural and industrial sectors (Zhang, Zeng, & Cheng, 2016). These sectors create effluents which include various pollutants such as metals, dyes, pharmaceuticals, herbicides, phenols, phosphate and nitrates (Reddy & Lee, 2013). Such contaminants are toxic and adversely affect organisms if exceed their allowable concentrations (Bhatnagar & Sillanpää, 2009). Therefore, the removal of these contaminants from wastewater is very important. Many techniques are adopted to treat aquatic pollutants such as adsorption, ion exchange, precipitation, membrane separation, electrochemical conversion and biodegradation (Sarode et al., 2019). Adsorption, for example, has been widely utilized due to its flexibility, low cost, high performance, efficient regeneration and eco-friendly operating system (Vakili et al., 2014).

Generally, there is a focus on using natural and renewable materials as cost-effective adsorbents in adsorption process. In this context, biosorbents gain wide attention owing to their quite abundance and non-toxic nature (Tran et al., 2015). Natural polymer biosorbents has been favorably utilized, in particular polysaccharides such as chitosan and its precursor chitin (Sarode et al., 2019). Chitin is the second naturally available biopolymer after cellulose. Crab and shrimp shells are the main sources of chitin (El Knidri, Belaabed, Addaou, Laajeb, & Lahsini, 2018). However, the poor solubility of chitin limits its application on a large-scale. Therefore, soluble chitosan has been derived from chitin by a process called alkaline deacetylation (Hamed, Özogul, & Regenstein, 2016; Muxika, Etxabide, Uranga, Guerrero, & de la Caba, 2017). Chitosan is an effective biosorbent towards a variety of contaminants due to its $-NH_2$ and $-OH$ groups enriched structure (Sharififard, Shahraki, Rezvanpanah, & Rad, 2018). However, chitosan showed poor mechanical strength and thermal resistance, weak stability and acid solubility and low surface area (Vakili et al., 2014).

Several modifications have been adopted to develop the properties of raw chitosan and chitin to resolve their limitations (El Knidri et al., 2018). Recently, chitosan/chitin-based composites are applied to adsorb various pollutants from wastewater. Oil palm ash (Hasan, Ahmad, & Hameed, 2008), biomass (Lessa, Nunes, & Fajardo, 2018), cellulose (Hu et al., 2019), clay (Auta & Hameed, 2014; Marrakchi, Khanday, Asif, & Hameed, 2016), resin (Lu et al., 2019), silica (Shan et al., 2019), zeolite (Khanday, Asif, & Hameed, 2017), synthetic polymer (Ghourbanpour, Sabzi, & Shafagh, 2019), bleaching earth clay (Islam, Tan, Islam, Romić, & Hameed, 2018), carbonaceous materials (Cui et al., 2019) and others (Abd Malek, Jawad, Abdulhameed, Ismail, & Hameed, 2020) are utilized to form composites with chitosan or chitin. Among these, incorporation of carbonaceous materials such as

* Corresponding author.
E-mail address: b.hammadi@qu.edu.qa (B.H. Hameed).

https://doi.org/10.1016/j.carbpol.2020.116690
Received 17 February 2020; Received in revised form 8 June 2020; Accepted 23 June 2020
Available online 28 June 2020

activated carbon (Karaer & Kaya, 2016), biochar (BC) (Liu, Zhou et al., 2019), carbon nanotubes (Abdel Salam, El-Shishtawy, & Obaid, 2014; Khakpour & Tahermansouri, 2018), graphene (Zhang, Chen, Guo, Zhu, & Zou, 2018) and graphene oxide (GO) (Wang, Yang et al., 2016) into chitin or chitosan structure exhibits composites with more stable structure, better pore properties and high adsorption performance.

Many published review articles have addressed the application of raw chitosan/chitin biopolymer and its derived adsorbents in treatment of many pollutants. These reviews mainly focused on biopolymer beads, membrane, fiber and film as well as cross-linked, grafted, impregnated and magnetic biopolymers (Ahmad, Manzoor, & Ikram, 2017; Bhatnagar & Sillanpää, 2009; Miretzky & Cirelli, 2009; Reddy & Lee, 2013; Sarode et al., 2019; Vakili et al., 2014; Wang, Wang et al., 2016; Zhang, Zeng et al., 2016). Moreover, review articles on incorporating of clay, synthetic polymer, iron oxide, biomass, alumina and cellulose to produce chitosan composites for wastewaters treatment were also reported (Olivera et al., 2016; Wan Ngah, Teong, & M.A.K.M., 2011). Some reviews also indicated the adsorption application of chitosan/chitin-carbonaceous material composites (Baig, Ihsanullah, & Saleh, 2019; Olivera et al., 2016; Vidal & Moraes, 2019; Wang, Guo, Qi, Liu, & Wei, 2019). However, the content of these reviews did not include detailed information about the preparation, modification, characteristics, adsorption application and regeneration of these adsorbents. Thus, this article is an up to date review of literature on the adsorption utilization of chitosan/chitin-carbonaceous material composites including the preparation and modification methods, characteristics, isotherms, kinetics, mechanisms and adsorption capacities. Regeneration capability of the reported adsorbents using various eluents was also discussed.

2. Chitosan and chitin

Natural biopolymers such as chitosan and chitin have been widely used in a variety of applications because of their low-cost, abundance and renewability (Hamed et al., 2016). Chitin is identified as the second naturally available biopolymer after cellulose, exists in the crab and shrimp shells, fungi and insects (González, Villanueva, Piehl, & Copello, 2015). N-acetyl glucosamine units mainly form the structure of chitin containing acetamido groups. Crustaceans represent a commercial source of chitin where about 1.2 million tons per year of the crustaceans waste in terms of exoskeleton is produced from food industry (Mo et al., 2018). The extraction of chitin from this solid waste solves the issue of waste treatment and prevents environmental contamination; providing a low-cost and sustainable raw material for synthesis of high-value polymeric matrices (Bakshi, Selvakumar, Kadirvelu, & Kumar, 2020; El Knidri et al., 2018).

Accordingly, chitosan biopolymer is derived from chitin by alkaline deacetylation process (Fig. 1). Chitosan has been used in many fields such as medicine, food, cosmetics and wastewater treatment (Auta & Hameed, 2013). This can be related to its favorable renewability, eco-friendly, active functional groups and biodegradability (Zhang, Luo, Liu, Fang, & Geng, 2016). Specifically, the existence of free $-NH_2$ and $-OH$ active groups confers chitosan structure an attractive characteristic in adsorption (Jawad, Norrahma, Hameed, & Ismail, 2019; Li et al., 2016). However, the drawbacks of chitosan are dissolution in acids, gelation in water and low surface area (Yadaei, Beyki, Shemirani, & Nouroozi, 2018). The preparation of chitosan/chitin-carbonaceous material composites can enhance the chemical stability, mechanical strength, surface area and adsorption performance of raw chitin or chitosan. These composites include activated carbon (Karaer & Kaya, 2016), biochar (Liu, Zhou et al., 2019), carbon nanotube (Abdel Salam et al., 2014; Khakpour & Tahermansouri, 2018) and graphene (Zhang et al., 2018) or graphene oxide (Wang, Yang et al., 2016).

3. Chitosan/chitin-carbonaceous materials composite

Biopolymers-based composites have received particular attention due to their environment friendly nature (Miretzky & Cirelli, 2011). Incorporation of carbonaceous materials into chitin/chitosan structure is an efficient way to improve its mechanical and thermochemical properties (Frindy et al., 2017; Sharififard et al., 2018). Moreover, these carbonaceous materials can improve the adsorption capability of biopolymers by enhancing its functionality and pore properties (Abdel Salam et al., 2014). Table 1 summarizes the pore characteristics of biopolymer-carbonaceous material composite adsorbents and their raw biopolymers. From this table, the carbonaceous materials have a significant role in the enhancement of pore properties of raw biopolymers. An overview on the percentage of published studies regarding the utilization of a specific carbonaceous material in the preparation of chitosan/chitin composite adsorbents shows that the most utilized carbonaceous materials are graphene oxide (44%) and activated carbon (24%) followed by carbon nanotubes (19%), biochar (7%) and graphene (6%). This section includes the preparation and modification methods along with properties of chitosan/chitin-carbonaceous material composites.

3.1. Chitosan/chitin-activated carbon composite

Activated carbon (AC) is a carbonaceous solid material with high surface area and adsorption capability. However, the properties of AC are mainly related to the used raw material and production technique (Ahmed & Hameed, 2019). Coconut shells, wood and coal represent common raw materials for commercial production of AC (Wong, Ngadi, Inuwa, & Hassan, 2018). Different precursors are used to prepare AC such as jackfruit peel (Foo & Hameed, 2012), coconut shell (Islam, Ahmed, Khanday, Asif, & Hameed, 2017), rattan (Islam, Ahmed, Khanday, Asif, & Hameed, 2017), palm date seed (Islam, Tan, Benhouria, Asif, & Hameed, 2015) and date stones (Foo & Hameed, 2011). Pyrolysis, chemical and/or physical activation are the main steps in AC production. The first step generates an intermediate product in terms of char which undergo the activation step to create AC with large surface area (Ahmed, 2017). Therefore, the total production cost of AC is relatively high. By its combination with chitosan or chitin few amounts of AC will be required in adsorption and treatment can be

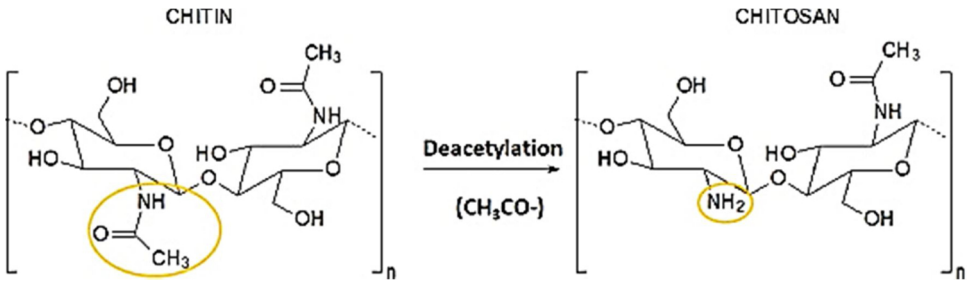

Fig. 1. Alkaline deacetylation of chitin to chitosan biopolymer.
(Reprinted with permission from Ref. (Muxika et al., 2017). Copyright 2017 Elsevier).

Table 1
Pore characteristics of some biopolymer-carbonaceous material composite adsorbents and their raw biopolymers.

Adsorbent	S_{BET} (m^2/g)	V_t (cm^3/g)	d_p (nm)	Reference
Chitosan-AC (M)	419.20	0.364	2.15	(Sharififard et al., 2018)
Chitosan	11.60	0.012	4.54	
Chitosan-AC	362.30	0.230	1.27	(Hydari et al., 2012)
Chitosan	16.37	0.019	4.49	
Chitosan-AC (M)	204.00	0.200		(Danalıoğlu et al., 2017)
Chitosan	61.00	0.096		
Chitosan-AC	147.85	0.227	7.32	(Banu et al., 2019)
Chitosan-AC (M)	123.84	0.068	2.60	(Karaer & Kaya, 2016)
Chitosan-BC (M)	134.68	0.054	2.05	(Xiao et al., 2019)
Chitosan-BC (M)	54.78	0.100	7.67	(Liu, Zhou et al., 2019)
Chitosan-BC	34.34	0.052	3.21	(Nitayaphat & Jintakosol, 2015)
Chitosan	2.63	0.031	3.55	
Chitosan -CNTs	104.00	1.220	14.30	(Khakpour & Tahermansouri, 2018)
Chitosan-CNTs (M)	70.90	0.025		(Neto et al., 2019)
Chitosan-CNTs	49.68	0.017		
Chitosan	25.20	0.009		
Chitosan-GO (M)	402.1	0.415	3.18	(Fan, Luo, Sun, Qiu et al., 2013)
Chitosan-GO (M)	388.30		13.98	(Wang, Yang et al., 2016)
Chitin-GO	186.98	1.027	16.75	(Song et al., 2019)
Chitin	146.02	0.881	17.49	
Chitosan-GO (M)	74.35	0.089	6.88	(Samuel et al., 2018)
Chitosan-GO (M)	54.71	0.044		(Hoa et al., 2016)
Chitosan	28.12	0.045		
Chitosan-GO	37.37		13.67	(Debnath et al., 2017)
Chitosan-G (M)	13.48	0.036	7.00	(Zhang et al., 2014)
Chitosan-G	1.03	0.003	12.60	(Mallakpour & Khadem, 2019)

S_{BET}: BET surface area; V_t: total pore volume; d_p: average pore size; AC: activated carbon; BC: biochar; CNTs: carbon nanotubes; GO: graphene oxide; G: graphene; M: magnetic.

turned to an economic and eco-friendly method (Hydari, Sharififard, Nabavinia, & Parvizi, 2012). Chitosan (CS) has a very low specific area within the range of 2–30 m^2/g whereas most of industrial ACs exhibit a range of 800–1500 m^2/g (Miretzky & Cirelli, 2009). However; micropores (pore size < 2 nm) enriched structure impedes the passage of adsorbates with molecular size larger than 2 nm such as rhodamine 6 G dye which may limit the utilization of ACs for large molecules adsorption (Wu, Xia, Cai, & Shi, 2018). CS-AC composite has a structure with favorable strength and porous structure (Yadaei et al., 2018).

CS-AC composite was commonly prepared as follows: AC was treated with oxalic acid for 4 h, filtered, rinsed with water and dehydrated at 70 °C for 12 h. CS mixed with oxalic acid under agitation at 40–45 °C to form CS gel. Acid treated AC was slowly added to the CS gel and agitated for 16 h at 40–45 °C. CS-AC composite was then obtained by dropwise addition of this mixture into NaOH precipitation medium (Hydari et al., 2012; Masih, Anthony, & Siddiqui, 2018). The composite was filtered, washed and dried at 50 °C. The produced CS-AC composite exhibited a surface area of 362.30 m^2/g relative to 16.32 m^2/g for CS (Table 1). Thus, the use of AC (922.33 m^2/g) favored the porous structure of composite. Moreover, the composite showed the peak for –NH bending vibrations of NH_2 group which characterized CS structure. Accordingly, CS-AC adsorbent had performance of about 5 times more than those of their individual components (Hydari et al., 2012).

A modified CS-AC composite in terms of magnetic structure was utilized as more developed adsorbent for water pollutants removal due to its highly chelating capability and easy magnetic separation (Danalıoğlu, Bayazit, Kuyumcu, & Abdel Salam, 2017; Yadaei et al., 2018). In this context, Karaer and Kaya (2016) obtained magnetic CS-AC composite as follows: CS was dissolved in acetic acid at room temperature for 12 h and then stirred at 60 °C for 30 min to make CS gel. Fe (III) (as $FeCl_3$) and Fe (II) (as $FeSO_4$) were dissolved and mixed with CS gel under stirring for 2 h. Acetic acid treated AC was added to the mixed solution and kept at 60 °C under stirring at 800 rpm for 3 h. The obtaining mixture was dropwise added into NaOH solution in order to make the composite (Fig. 2). The magnetic CS-AC composite showed high surface area of 123.84 m^2/g and high adsorption capacity towards dyes. Li et al. (2017) reported that the magnetic composite in terms of Fe_3O_4 modified CS-AC composite (FeCS-AC) exhibited an adsorption performance towards Cu^{2+} ions of 10% higher than that of raw CS-AC, even though surface area of FeCS-AC was only 27.97 m^2/g, lower than that of CS-AC with 107.59 m^2/g. This could be related to the favorable role of Fe-O group in attraction of Cu^{2+} ions.

3.2. Chitosan/chitin-biochar composite

Biochar is a porous carbon obtained by carbonization of biowastes under limited oxygen atmosphere (Han et al., 2019). It can be used as a catalyst precursor, soil amendment as well as a good adsorbent for various contaminates owing to its porous structure and active functional groups (Zhang, Zhu, Shen, & Liu, 2019). Development of chitosan/chitin–biochar composites has been reported in some studies (Afzal et al., 2018; Nitayaphat & Jintakosol, 2015; Xiao et al., 2019; Zhang, Tang et al., 2019). The addition of biopolymer to biochar is an efficient way to merge and improve the characteristics of both solids. In this composite, the biochar acts as a perfect support owing to its favorable structure in terms of high surface area and enriched active groups, while the CS acts as the source of chelating sites to pollutant molecules due to its $–NH_2$ and $-OH$ groups (Zhang, Tang et al., 2019). Chitosan-biochar composites were found to be effective adsorbents for treatment of inorganic and organic pollutants (Afzal et al., 2018; Xiao et al., 2019).

Chitosan-biochar composite was prepared by mixing of biochar and chitosan with 50 mL of 2% (v/v) acetic acid and agitation for 3 h at 30 °C. The sample was then injected from a syringe into an alkaline precipitation medium in order to form the composite. The surface area, total pore volume and average pore width of chitosan-biochar composite were 34.34 m^2/g, 0.052 cm^3/g and 3.21 nm relative to 2.63 m^2/g, 0.031 cm^3/g and 3.55 nm for original chitosan (Table 1). The presence of biochar in composite was significantly enhanced the surface area and pore volume and reduced the pore width of raw chitosan. The surface area of composite was 13 times more than that of chitosan which resulted in 97% enhancement in adsorption performance (Nitayaphat & Jintakosol, 2015).

Although, the chitosan-biochar composite showed better adsorption

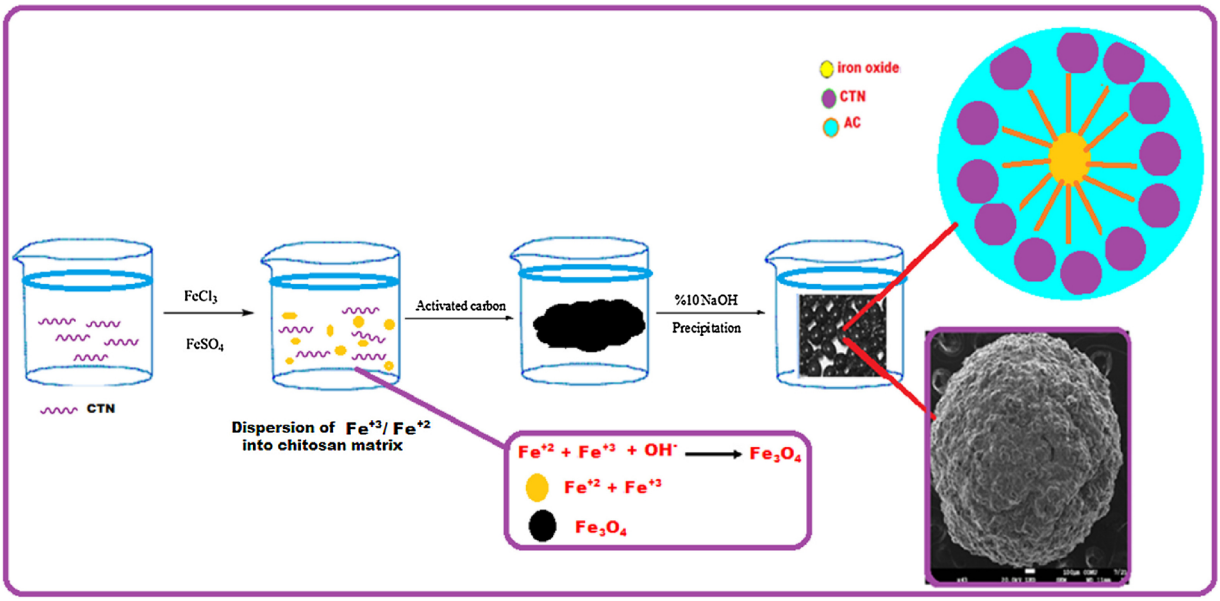

Fig. 2. Schematic illustration of the synthesis of magnetic chitosan-AC composite.
(Reprinted with permission from Ref. (Karaer & Kaya, 2016). Copyright 2016 Elsevier).

properties relative to chitosan, the composite was difficult to separate from aqueous solution. Many studies have focused on developing magnetic adsorbents with best separation and more ability to treat pollutants. Xiao et al. (2019) reported that $FeCl_3$ modified biochar-chitosan composite exhibited adsorption performances towards Cr(VI) and Cu(II) of 26% and 18% higher than the original biochar-chitosan composite. $FeCl_3$ provided additional active groups in the composite structure which enhanced the removal of Cr(VI) and Cu(II) by the interaction mechanisms of physical adsorption and precipitation, surface complexation and ion exchange.

3.3. Chitosan/chitin-carbon nanotubes composite

Carbon nanotubes (CNTs) are a new type of carbonaceous materials that gained wide attention since the first time of preparation in 1991 (Iijima, 1991). These materials have high surface area and best thermochemical properties (Sarkar et al., 2018). However, the agglomeration tendency and poor structural groups of CNTs limits their adsorption application (Fiyadh et al., 2019). Incorporation of biopolymer to CNTs is considered as the best way to overcome the weakness of the CNTs (Dou et al., 2019). Chitosan imparts CNTs a good dispersing tendency and active groups in terms of $–NH_2$. Therefore, such composite can be a perfect adsorbent for wastewater treatment (Parlayıcı & Pehlivan, 2019). Chitosan/chitin-CNTs composites have been adopted as efficient adsorbents with high performance (Abdel Salam et al., 2014; Huang et al., 2018). Moreover, the addition of CNTs into biopolymers also greatly enhances mechanical properties of biomaterials (Zhu, Jiang, Xiao, & Zeng, 2010).

For synthesis of CS-CNTs composite, CS was first dissolved in 500 mL of 2% (v/v) acetic acid solution and then mixed with CNTs. The formed sample was sonicated for 20 min and then agitated for 1 h until the formation of a uniform solution. Secondly, the solution was adjusted to a pH of 11 with the aid of ammonia (1% v/v) and heated to 60 °C for further 1 h. Then, 1 mL of glutaraldehyde (GLA) was added into the reactants for cross-linking of CS under agitation for another 1 h. Finally, CS-CNTs composite was filtered, washed and dried at 70 °C overnight (Khakpour & Tahermansouri, 2018). According to published studies, GLA is a common crosslinking agent used to enhance the chitosan stability under acidic medium. GLA molecule contains two aldehyde functional groups which react with amino groups of chitosan to form cross-linked structure. In the CS-CNTs composite, the oxygen-contained functional groups of CNTs interact with amino groups of CS, as shown in Fig. 3. GLA represents a toxic substance and may pose a big threat to the aqua ecosystem. The long-term exposure to GLA at concentration of about 2.5 ppm will decrease the reproduction rate of fishes to as high as 97% (Sano, Krueger, & Landrum, 2005). Despite the toxicity of GLA, the substance is still widely used for crosslinking of chitosan when used as an adsorbent material (Vakili et al., 2014). The application of magnetic adsorbent technology can ensure sufficient recovery of adsorbent from treated water and thereby it can solve the environmental problems associated with the use of toxic adsorbents (Fan, Luo, Sun, Li, & Qiu, 2013).

The introducing of the most common magnetic materials such as Fe_3O_4 or Fe_2O_3 into a biopolymer-CNTs composite will combine the high adsorption capacity of composite and the separation convenience of magnetic materials (Fig. 4). Thus, magnetic chitosan/ chitin-CNTs composites have attracted the attention of many researchers as more easily separated adsorbents with high adsorption performances towards organic and inorganic pollutants (Abdel Salam et al., 2014; Wang et al., 2015; Zhu et al., 2010). The iron oxide presents a large number of active sites for adsorption and relatively develops the porous structure of the adsorbent. Neto, Bellato, and Silva (2019) showed that the Fe_3O_4 modified CS-CNTs composite exhibited a surface area of 70.90 m^2/g and pore volume of 0.025 cm^3/g relative to 49.68 m^2/g and 0.017 cm^3/g for original CS-CNTs composite (Table 1). Moreover, Fe_3O_4 modified CS-CNTs composite showed high adsorption performance towards Cr (VI) owing to the electrostatic and ion exchange interaction mechanisms between iron oxide and metal ions. This confirms the role of Fe_3O_4 in development of porous structure of CS-CNTs composite.

3.4. Chitosan/chitin-graphene/GO composite

Graphene is an emerging form of carbonaceous materials which has promising thermal, electrical and mechanical characteristics. It also has a large specific area (2630 m^2/g) which renders it as an efficient adsorbent (Zhang et al., 2014). However, graphene is easy to agglomerate in aqueous solution, causing a decrease in its surface area. Graphene nanoparticle cannot recover or reuse and may act as a pollutant, which restricts its adsorption applications (Li, Liu, Zeng, Liu, & Liu, 2019). GO is derived from graphite according to the common Hummers or some developed techniques. By these techniques, graphite is first oxidized to

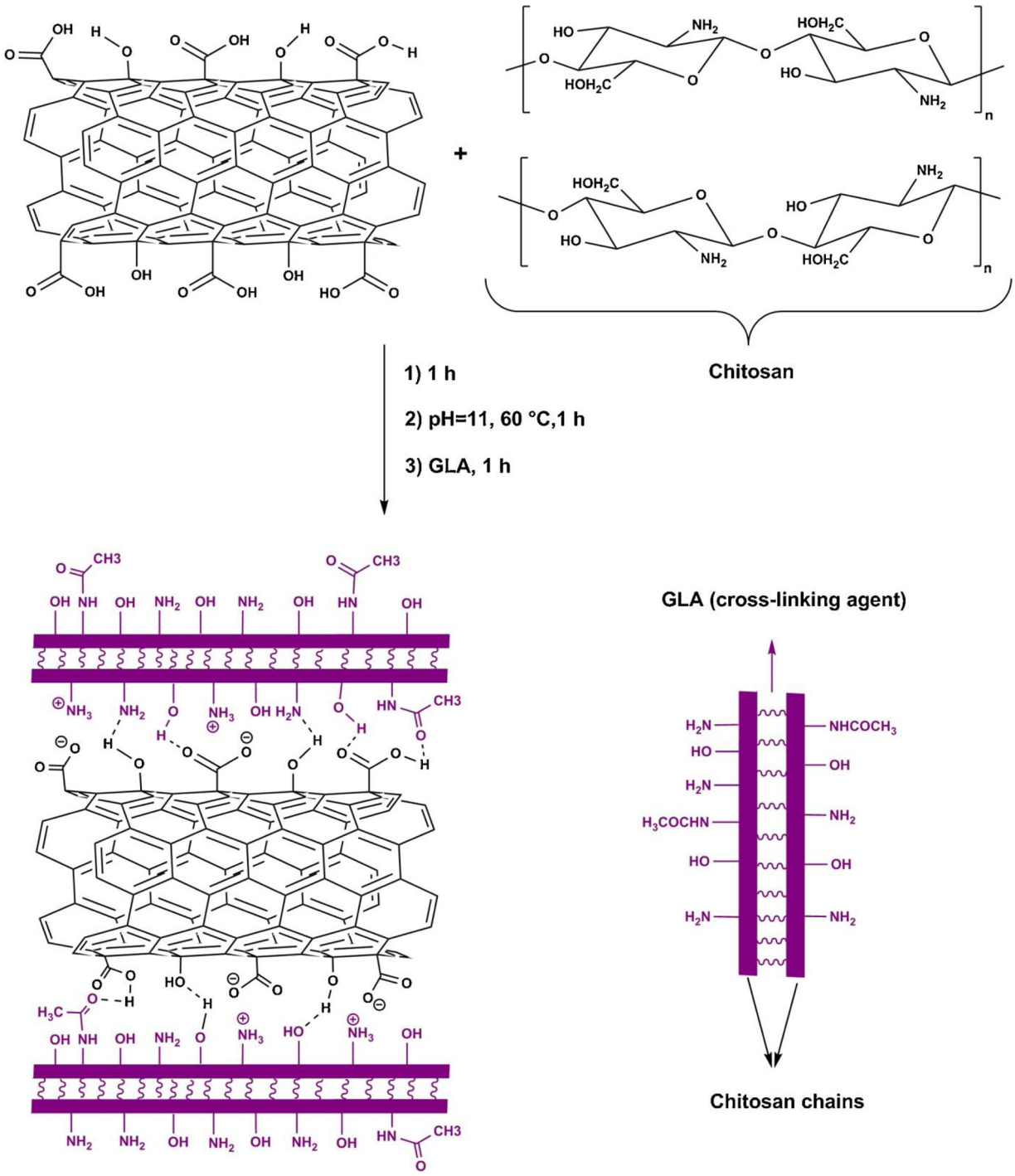

Fig. 3. The modification route of CNTs by chitosan.
(Reprinted with permission from Ref. (Khakpour & Tahermansouri, 2017). Copyright 2017 Elsevier).

graphite oxide which is then exfoliated to GO (Peng, Li, Liu, & Song, 2017). GO has many active structural groups; however, its high dispersibility, agglomeration tendency and low recovery limit its adsorption applications (Sherlala, Raman, Bello, & Asghar, 2018). Incorporation of GO to other materials can improve its characteristics and performance. For instance, GO/graphene-biopolymer composites have shown favorable structure and high adsorption capacity (Ma et al., 2016; Salzano de Luna et al., 2019; Zhang et al., 2018). In the composite (Fig. 5), the −COOH of GO interacts with the $–NH_2$ of biopolymer through hydrogen bonding and electrostatic mechanisms (Kumar & Jiang, 2016). CS-GO composite, CS and GO adsorbents exhibited adsorption capacities of 216.92, 180.18 and 98.33 mg/g for palladium metal, respectively. Thus, CS-GO composite has adsorption performance higher than either of its individual constituents. This could be related to the high surface area of GO and highly active groups of CS biopolymer (Liu et al., 2012). Similar results were reported by Hydari et al. (2012) for CS-AC composite. The adsorption capacities of cadmium on CS-AC, AC and CS were 52.63, 10.3 and 10.0 mg/g, respectively.

The modification of GO-biopolymer composite by magnetic materials such as Fe_3O_4 (Fig. 6) or Fe_2O_3 provided additional properties in terms of stability, low toxicity, easy separation and reutilization

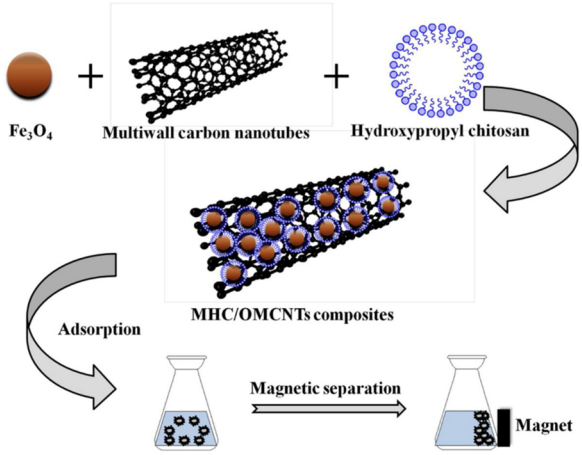

Fig. 4. The application of magnetic chitosan-CNTs composite for removal of lead ions with the help of external magnetic field.
(Reprinted with permission from Ref. (Wang et al., 2015). Copyright 2015 Elsevier).

(Samuel, Shah, Bhattacharya, Subramaniam, & Pradeep Singh, 2018). Thus, magnetic GO/graphene-biopolymer composites were adopted for application in the removal of dyes (Gul et al., 2016), metals (Subedi, Lähde, Abu-Danso, Iqbal, & Bhatnagar, 2019) and drugs (Huang et al., 2017).

From Section 3, it can be deduced that the incorporation of carbonaceous materials including graphene oxide, activated carbon, carbon nanotube and biochar into the chitosan/chitin can improve the structure of chitosan/chitin by combining the high surface area of carbonaceous material and the active functional groups of chitosan/chitin. Accordingly, chitosan/chitin-carbonaceous material composites show higher adsorption performance than raw chitosan/chitin and in some cases exceed the adsorption performance of carbonaceous material. Table 1 confirms the developed porous structure of biopolymer-carbonaceous materials composite relative to its raw biopolymer. For instance, the surface area and pore volume of chitosan-AC composite are 22 and 12 times more than those of raw chitosan, respectively. This table also shows that activated carbon and graphene oxide exhibit biopolymer composites with the highest surface areas relative to other carbonaceous materials. Moreover, the magnetic composite can be a more developed adsorbent in terms of improved adsorption capacity

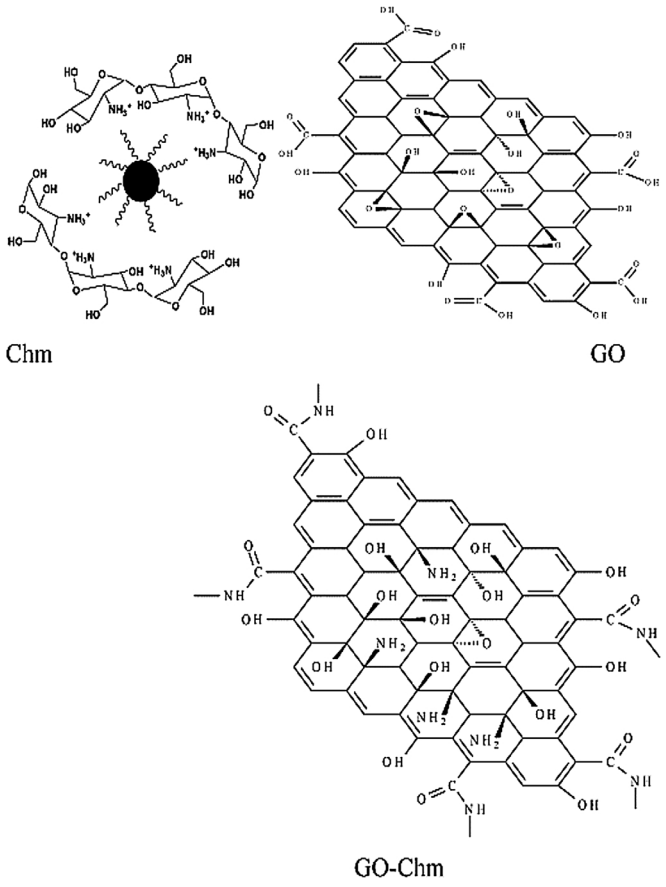

Fig. 6. Proposed synthesis of chitosan-GO composite.
(Reprinted with permission from Ref. (Shah et al., 2018). Copyright 2018 Elsevier).

and efficient separation. This can be related to the favorable role of magnetic materials such as Fe_3O_4 or Fe_2O_3 in improvement of composite structure either by the enhancement of surface area (Table 1) or inserting of additional active groups and providing of magnetic property.

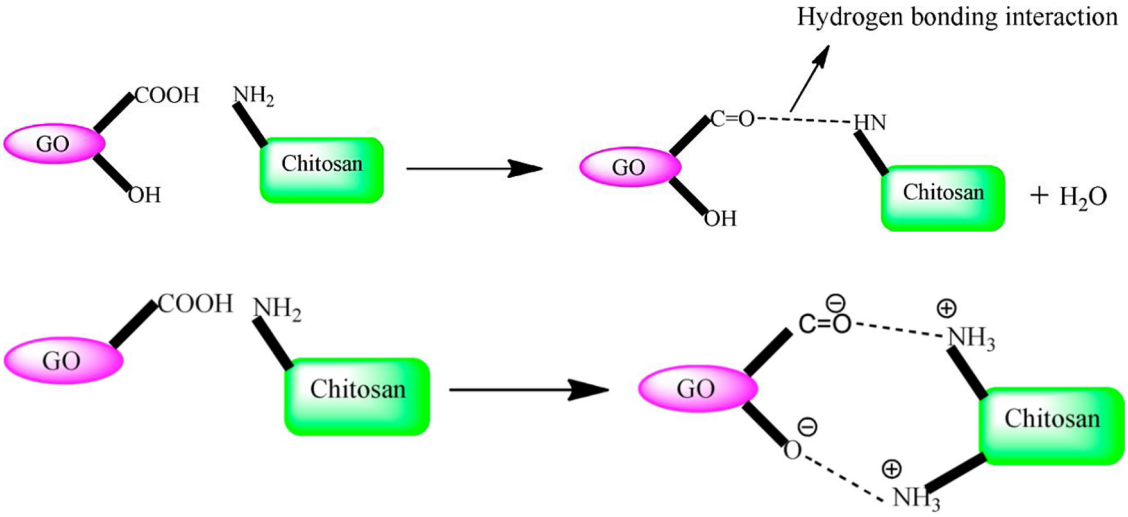

Fig. 5. Hydrogen-bonding & ion pair interaction mechanisms between GO and chitosan.
(Reprinted with permission from Ref. (Kumar & Jiang, 2016). Copyright 2016 Elsevier).

Table 2
Adsorption properties of metal ions removal using different chitosan/chitin-based composites.

Adsorbent	Metal	Isotherm conditions	q_{max} (mg/g)	Isotherm	Kinetic	Reference
Chitosan-AC	Cu(II)	0.5 g/L, 25 °C, 3 h, pH 5, 50 – 600 mg/L	490.40	Freundlich	PSO	(Dandil et al., 2019)
Chitosan-AC	Cd(II)	2 g/L, 25 °C, 0.67 h, pH 5, 15 – 200 mg/L	357.14	Langmuir, Freundlich		(Rahmi & Nurfatimah, 2018)
Chitosan-AC (M)	Cd(II)	0.5 g/L, 25 °C, 24 h, pH 6, 5 – 300 mg/L	344.0	Langmuir	PSO	(Sharififard et al., 2018)
Chitosan-AC (M)	Cd(II)	0.65 g/L, rT °C, 1 min, pH 8, 0.5 – 150 mg/L	251.9	Redlich-Peterson	PSO	(Yadaei et al., 2018)
Chitosan-AC (M)	Cu(II)	0.1 g/L, 25 °C, 2 h, pH 5.5, 0 – 1000 mg/L	216.61	Langmuir	PSO	(Li et al., 2017)
Chitosan-AC	Cu(II)	1 g/L, 20 °C, 24 h, pH 7, 1 – 10 mg/L	90.91	Langmuir	PSO	(Masih et al., 2018)
Chitosan-AC	Cd(II)	4 g/L, rT °C, 24 h, pH 6, 10 – 50 mg/L	52.63	Langmuir	PSO	(Hydari et al., 2012)
Chitosan	Cd(II)	4 g/L, rT °C, 24 h, pH 6, 10 – 50 mg/L	10.0	Langmuir	PSO	
Chitosan-BC	Pb(II)	3.3 g/L, 25 °C, 15 h, pH 5, 0 – 400 mg/L	476.19	Langmuir	PSO	(Zhang, Tang et al., 2019)
Chitosan-BC	Cd(II)	3.3 g/L, 25 °C, 15 h, pH 5, 0 – 400 mg/L	370.37	Langmuir, Freundlich	PSO	(Zhang, Tang et al., 2019)
Chitosan-BC	Cr(III)	3.3 g/L, 25 °C, 15 h, pH 5, 0 – 400 mg/L	312.50	Langmuir	PSO	(Zhang, Tang et al., 2019)
Chitosan-BC	Zn(II)	3.3 g/L, 25 °C, 15 h, pH 5, 0-400 mg/L	114.94	Langmuir	PSO	(Zhang, Tang et al., 2019)
Chitosan-BC	Cu(II)	3.3 g/L, 25 °C, 15 h, pH 5, 0 – 400 mg/L	111.11	Langmuir	PSO	(Zhang, Tang et al., 2019)
Chitosan-BC	Ni(II)	3.3 g/L, 25 °C, 15 h, pH 5, 0 – 400 mg/L	99.01	Langmuir	PSO	(Zhang, Tang et al., 2019)
Chitosan-BC (M)	Cu(II)	0.5 g/L, 30 °C, 18 h, pH 5.8, 0 – 40 mg/L	54.68		PSO	(Xiao et al., 2019)
Chitosan-BC	Ag(I)	10 g/L, 30 °C, 3 h, pH 6, 1 – 10 mg/L	52.91	Langmuir		(Nitayaphat & Jintakosol, 2015)
Chitosan	Ag(I)	10 g/L, 30 °C, 3 h, pH 6, 1 – 10 mg/L	26.88	Langmuir		
Chitosan-BC (M)	Cr(VI)	0.5 g/L, 30 °C, 18 h, pH 3, 0 – 40 mg/L	30.14		PSO	(Xiao et al., 2019)
Chitosan-CNTs (M)	Cr(VI)	0.3 g/L, 25 °C, 3 h, pH 4, 50 – 700 mg/L	449.30	Langmuir	PSO	(Neto et al., 2019)
Chitosan-CNTs	Cr(VI)	1 g/L, 40 °C, 24 h, pH 2, 50 – 600 mg/L	163.93	Langmuir	PSO	(Huang et al., 2018)
Chitosan-CNTs (M)	Pb(II)	0.4 g/L, 25 °C, 2 h, pH 5, 10 – 200 mg/L	116.30	Sips	PSO	(Wang et al., 2015)
Chitosan-CNTs	Cu(II)	0.2 g/L, 25 °C, 1 h, pH 7, 5 – 40 mg/L	115.84	Langmuir	PSO	(Dou et al., 2019)
Chitosan-CNTs	Pb(II)	1 g/L, 25 °C, 1 h, pH 2, 20 – 100 mg/L	83.20	Langmuir	PSO	(Wang et al., 2020)
Chitosan-CNTs (M)	Cr(III)	0.3 g/L, 25 °C, 3 h, pH 4, 5 – 100 mg/L	66.25	Langmuir	PSO	(Neto et al., 2019)
Chitosan-CNTs	Cr(VI)	1 g/L, 35 °C, 2 h, pH 6, 0 – 25 mg/L	26.14	Langmuir	PSO	(Parlayıcı & Pehlivan, 2019)
Chitosan-GO	Pb(II)	1 g/L, 20 °C, 1.5 h, pH 5, 10 – 500 mg/L	447.0	Freundlich	PSO	(Li et al., 2015)
Chitosan-GO	Cu(II)	1 g/L, 20 °C, 1.5 h, pH 5, 10 – 500 mg/L	425.0	Freundlich	PSO	(Li et al., 2015)
Chitosan-GO	Pb(II)	0.1 L, 30 °C, 11 h, pH 5, 25 – 600 mg/L	392.2	Langmuir	PSO	(Luo et al., 2019)
Chitosan-GO	Ag(I)	0.1 L, 30 °C, 11 h, pH 5, 25 – 600 mg/L	255.8	Langmuir	PSO	(Luo et al., 2019)
Chitosan-GO	Pd(II)	2 mg, 30 °C, 16 h, pH 3, 10 – 100 mg/L	216.93	Langmuir	PSO	(Liu et al., 2012)
Chitosan-GO	Cu(II)	0.1 L, 30 °C, 11 h, pH 5, 25 – 600 mg/L	146.4	Langmuir	PSO	(Luo et al., 2019)
Chitosan-GO (M)	Cd(II)	1 g/L, 20 °C, 1.5 h, pH 5, 10 – 500 mg/L	177.0	Freundlich	PSO	(Li et al., 2015)
Chitosan-GO (M)	Cr(VI)	1 g/L, 25 °C, 1.5 h, pH 2, 20 – 100 mg/L	140.84	Freundlich	PSO	(Zhang, Luo et al., 2016)
Chitosan-GO (M)	Pb(II)	1 g/L, 27 °C, 24 h, pH 5, 10 – 150 mg/L	112.35	Langmuir	PSO	(Samuel et al., 2018)
Chitosan-GO	Cu(II)	1.2 g/L, 30 °C, 3 h, pH 3, 20 – 100 mg/L	111.11	Langmuir	PSO	(Anush et al., 2019)
Chitosan	Cu(II)	1.2 g/L, 30 °C, 3 h, pH 3, 20 – 100 mg/L	9.70	Langmuir	PSO	
Chitosan-GO	Cr(VI)	0.25 g/l, 27 °C, 7 h, pH 2, 10 – 125 mg/L	104.16	Langmuir	PSO	(Samuel et al., 2019)
Chitosan-GO (M)	Cr(VI)	0.5 g/L, 22 °C, 3 h, pH 2, 10 – 100 mg/L	100.51	Freundlich	PSO	(Subedi et al., 2019)
Chitosan-GO (M)	Pb(II)	0.8 g/L, 30 °C, 1 h, pH 5, 8 – 55 mg/L	76.94	Langmuir	PSO	(Shah et al., 2018)
Chitosan-GO	Cr(VI)	1.2 g/L, 30 °C, 3 h, pH 3, 20 – 100 mg/L	76.92	Langmuir	PSO	(Anush et al., 2019)
Chitosan-GO	As(V)	8 g/L, 30 °C, 1 h, pH 5.5, 30 – 500 mg/L	71.90	Freundlich, Langmuir	PSO	(Kumar & Jiang, 2016)
Chitosan-GO	Cu(II)	0.63 g/L, 30 °C, 24 h, pH 6, 1.9 – 32.0 mg/L	25.4	Langmuir	PSO	(Yu et al., 2013)
Chitosan-G (M)	Hg(II)	0.12 g/L, 50 °C, 5 h, pH 7, 5 – 100 mg/L	361.0	Langmuir	PSO	(Zhang et al., 2014)
Chitosan-G	Cd(II)	2 g/L, 25 °C, 24 h, pH 6, 20 – 80 mg/L	35.0	Langmuir, Freundlich	PSO	(Mallakpour & Khadem, 2019)

AC: activated carbon, BC: biochar, CNTs: carbon nanotubes, GO: graphene oxide, G: graphene, M: magnetic, q_{max}: maximum uptake.

4. Adsorption application of chitosan/chitin-based composites

Adsorption is basically defined as a separation process which includes the accumulation of a liquid or gaseous adsorbate at the surface and the inter pores of a solid adsorbent (Garba et al., 2019). This process has been identified as a highly efficient, simple, low-cost and eco-friendly wastewaters treatment technique (Khanday, Ahmed, Okoye, Hummadi, & Hameed, 2019). Adsorption performance mainly depends on adsorbent type and adsorption conditions (e.g. temperature, time, pH, concentration, etc). In this regard, chitosan/chitin-based adsorbents in terms of composites with carbonaceous materials have been used for treatment of water contaminants owing to their high efficiency, best chemical and mechanical stability and favorable porous structure (Dandil, Sahbaz, & Acikgoz, 2019; González, Bafico, Villanueva, Giorgieri, & Copello, 2018). The maximum adsorption capacities of chitosan/chitin-carbonaceous material composites towards heavy metals, dyes and other pollutants such as pharmaceuticals, herbicides, phenols, nitrates and phosphates under specified adsorption conditions are presented in Tables 2–4, respectively. Moreover, the most widely used isotherm models, kinetic models, and error functions are presented in Table S1 (supplementary data).

4.1. Heavy metals

Heavy metals are recognized as dangerous pollutants because of their non-biodegradable and toxic nature. These pollutants can be found in effluents of batteries, mining, fertilizer and painting industries (Vakili et al., 2019). According to the collected data (Table 2), the most widely tested heavy metal ions are copper, chromium, cadmium and lead. This can be related to the high benefits in regaining of these metals and avoiding of their high dangerous level once present in water (Wong et al., 2018). For example, copper dosage of greater than 1.3 mg/L affects human organs and causes cancer. Cadmium can impact the human liver. Chromium is highly harmful to humans due to its carcinogenic effect. Lead results in cancer and even death (Ahmed & Hameed, 2019). Thus, many studies were addressed the adsorption of metal ions on chitin/chitosan-carbonaceous material composites.

Li et al. (2017) explored the copper (II) adsorption on magnetic chitosan-activated carbon (CS-AC) composite. Isotherm data showed that Langmuir model exhibited a determination coefficient R^2 of 0.957 compared to R^2 of 0.888 and 0.942 for Freundlich and Temkin models, respectively. Regarding kinetic data, pseudo-second order (PSO) model showed R^2 of 0.990 compared to R^2 of 0.974 and 0.980 for pseudo-first order (PFO) and Elovich models. Thus, the adsorption data followed the Langmuir and PSO equations, suggesting a monolayer coverage and

Table 3
Adsorption properties of synthetic dyes removal using different chitosan/chitin-based composites.

Adsorbent	Dye	Isotherm conditions	q_{max} (mg/g)	Isotherm	Kinetic	Reference
Chitosan-AC	Acid blue 29	1 g/L, 50 °C, 3.3 h, pH 7, 50 – 350 mg/L	596.4	Langmuir	PSO	(Auta & Hameed, 2013)
Chitosan	Acid blue 29	1 g/L, 50 °C, 3.3 h, pH 7, 50 – 350 mg/L	376.9	Langmuir	PSO	
Chitosan-AC (M)	Methylene blue	1 g/L, 45 °C, 24 h, pH 7.73, 50 – 500 mg/L	500.0	Langmuir	PSO	(Karaer & Kaya, 2016)
Chitosan-AC	Methylene blue	1 g/L, 50 °C, 3.3 h, pH 7, 50 – 350 mg/L	388.1	Langmuir	PSO	(Auta & Hameed, 2013)
Chitosan	Methylene blue	1 g/L, 50 °C, 3.3 h, pH 7, 50 – 350 mg/L	234.5	Langmuir	PSO	
Chitosan-AC (M)	Reactive blue 4	1 g/L, 45 °C, 24 h, pH 7.73, 50 – 500 mg/L	250.0	Langmuir	PSO	(Karaer & Kaya, 2016)
Chitosan-AC	Crystal violet	10 g/L, 70 °C, 2 h, pH 9, 20 – 100 mg/L	12.50	Langmuir	PSO	(Kumari et al., 2017)
Chitosan-AC	Malachite green	5 g/L, 50 °C, 1 h, pH 4, 70 mg/L	4.80	Langmuir	PSO	(Arumugam et al., 2019)
Chitosan-CNTs	Congo red	20 g/L, 30 °C, 24 h, pH 5, 10 – 1000 mg/L	450.4	Langmuir	PFO	(Chatterjee et al., 2010)
Chitosan-CNTs (M)	Methyl orange	0.6 g/L, 24 °C, 2 h, pH 6.5, 5 – 50 mg/L	66.09	Langmuir	PSO	(Zhu et al., 2010)
Chitosan-CNTs	Direct blue 7	1 g/L, rT °C, 6 h, pH 6, 10 – 80 mg/L	29.33	Langmuir		(Abbasi & Habibi, 2016)
Chitin-CNTs (M)	Rose Bengal	0.2 g/L, 25 °C, 2 h, pH 8, 5 mg/L	6.25	–	PSO	(Abdel Salam et al., 2014)
Chitosan-GO (M)	Rhodamine B	0.12 g/L, 35 °C, 0.08 h, pH 6.5, 50 – 250 mg/L	1085.3	Langmuir	PSO	(Marnani & Shahbazi, 2019)
Chitosan-GO	Methylene blue	0.2 g/L, 30 °C, 24 h, pH 7, 0 – 300 mg/L	1023.9	Langmuir	PSO	(Yan et al., 2019)
Chitosan-GO	Metanil yellow	0.17 g/L, 30 °C, 1.5 h, pH 6.8, 20 – 600 mg/L	558.18	Langmuir	PSO PFO	(Lai, Hiew et al., 2019)
Chitosan-GO	Methyl orange	0.5 g/L, 25 °C, 24 h, pH 4, 20 – 800 mg/L	398.08	Langmuir	PSO	(Jiang et al., 2016)
Chitosan-GO	Safranin O	0.5 g/L, 35 °C, 1 h, pH 6.5, 25 – 600 mg/L	330.60	Langmuir	PFO	(Debnath et al., 2017)
Chitosan-GO (M)	Methylene blue	2 g/L, 25 °C, 1 h, pH 9, 10 – 150 mg/L	249.23	Langmuir	PSO	(Hoa et al., 2016)
Chitin-GO	Methylene blue	0.4 g/L, 30 °C, 6 h, pH 7, 12 – 108 mg/L	173.3	Langmuir		(Ma et al., 2016)
Chitin-GO	Neutral red	1 g/L, 25 °C, 24 h, pH 5, 0.025 – 7 mmol/L	165.0	Sips	PFO	(González et al., 2015)
Chitin	Neutral red	1 g/L, 25 °C, 24 h, pH 5, 0.025 – 7 mmol/L	17.04	Sips	PFO	
Chitosan-GO	Fuchsin acid	0.5 g/L, 20 °C, 13 h, pH 3, 50 – 150 mg/L	163.93	Langmuir	PSO	(Li et al., 2014)
Chitosan-GO	Methylene blue	0.4 g/L, 25 °C, 1.3 h, pH 11, 20 – 160 mg/L	84.32	Langmuir	PSO	(Fan, Luo, Sun, Qiu et al., 2013)
Chitosan	Methylene blue	0.4 g/L, 25 °C, 1.3 h, pH 11, 20 – 160 mg/L	50.12	Langmuir	PSO	
Chitin-GO	Remazol black	1 g/L, 25 °C, 24 h, pH 4, 0.025 – 5 mmol/L	70.0	Sips	PFO	(González et al., 2015)
Chitosan-GO (M)	Methyl violet	1 g/L, 25 °C, 1 h, pH 10, 2 – 30 μg/L	17.66	Langmuir	PSO	(Gul et al., 2016)
Chitosan-GO (M)	Alizarin yellow R	1 g/L, 25 °C, 1.3 h, pH 6, 2 – 30 μg/L	13.32	Langmuir	PSO	(Gul et al., 2016)
Chitosan-G	Congo red	0.5 g/L, 25 C, 0.17 h, pH 7, 5 – 500 mg/L	384.62	Langmuir	PSO	(Omidi & Kakanejadifard, 2018)
Chitosan-G	Methyl orange	16 g/L, 25 °C, 2 h, pH 3, 20 – 80 mg/L	230.91	Freundlich	PSO	(Zhang et al., 2018)
Chitosan-G	Acid red	16 g/L, 25 °C, 2 h, pH 4, 10 – 60 mg/L	132.94	Freundlich	PSO	(Zhang et al., 2018)

AC: activated carbon, BC: biochar, CNTs: carbon nanotubes, GO: graphene oxide, G: graphene, M: magnetic, q_{max}: maximum uptake.

rate-limiting chemisorption step (Huang et al., 2018). The values of separation factor R_L (0.047 – 0.831) were between 0 and 1 suggested favorable adsorption (Yadaei et al., 2018). The saturated uptake was reported as 216.6 mg/g. The adsorbed amount at 5 min attained 77% of the equilibrium uptake at 120 min. Initially, the abundance of active sites resulted in a rapid Cu^{2+} attraction. This was followed by a slow attraction as a result of occupation of active sites and then reached equilibrium (Zhang, Luo et al., 2016). The more developed pores of composite were greatly improved the performance and rate of adsorption. The results revealed that $–NH_2$ and $-OH$ groups were significantly chelated metal ions. The adsorption capacity of magnetic CS-AC for Cu^{2+} was increased from 72 to 117 mg/g with initial pH changing from 4.0 to 5.5 and reduced to 96 mg/g at an initial pH of 6.0. This could be related to the precipitation of Cu^{2+} hydroxide precipitate at higher initial pH values (Dou et al., 2019). Moreover, the results showed that the magnetic CS-AC composite exhibited an adsorption capacity for Cu^{2+} ions of 10% higher than that of raw CS-AC due to the role of Fe-O group in attraction of Cu^{2+} ions.

Table 4
Adsorption properties of other pollutants removal using various chitosan/chitin-based composites.

Adsorbent	Pollutant	Isotherm conditions	q_{max} (mg/g)	Isotherm	Kinetic	Reference
Chitosan-AC (M)	Amoxicillin	0.1 g/L, 25 °C, 2 h, 5 – 60 mg/L	526.31	Langmuir	PSO	(Danalıoğlu et al., 2017)
Chitosan-AC	Phenol	5 g/L, 28 °C, 1 h, pH 4, 20 – 800 mg/L	409.0	Freundlich	PSO	(Soni et al., 2017)
Chitosan-AC (M)	Erythromycin	0.1 g/L, 25 °C, 2 h, 5 – 60 mg/L	178.57	Langmuir	PSO	(Danalıoğlu et al., 2017)
Chitosan-AC	Phosphate	2 g/L, 30 °C, 0.5 h, pH 5.3, 5 – 300 mg/L	131.29	Freundlich	PSO	(Banu et al., 2019)
Chitosan-AC (M)	Ciprofloxacin	0.1 g/L, 25 °C, 2 h, 5 – 60 mg/L	90.10	Freundlich	PSO	(Danalıoğlu et al., 2017)
Chitosan-AC	Nitrate	2 g/L, 30 °C, 0.75 h, pH 6.4, 5 – 300 mg/L	90.09	Freundlich	PSO	(Banu et al., 2019)
Chitosan-C (M)	Phosphate	2 g/L, 28 °C, 24 h, pH 5, 5 – 200 mg/L	62.72	Langmuir	PSO	(Cui et al., 2019)
Chitosan-C (M)	Nitrate	2 g/L, 28 °C, 24 h, pH 3, 1 – 200 mg/L	41.90	Langmuir	Elovich	(Cui et al., 2019)
Chitosan-BC (M)	Tetracycline	1 g/L, 35 °C, 12 h, pH 5, 100 – 1000 mg/L	210.95	Sips	PSO	(Liu, Zhou et al., 2019)
Chitosan-BC	Ciprofloxacin	5 g/L, 30 °C, 24 h, pH 3, 5 – 160 mg/L	78.79	Langmuir	PSO	(Afzal et al., 2018)
Chitosan-CNTs	Tri-nitrophenol	0.3 g/L, 25 °C, 4 h, pH 7, 10 – 100 mg/L	666.67	Langmuir, Freundlich	PSO	(Khakpour & Tahermansouri, 2018)
Chitosan-CNTs	Phenol	0.05 g/L, 25 °C, 2 h, pH 6.5, 50 – 400 mg/L	404.2	Dubinin-Radushkevic	PSO	(Alves et al., 2019)
Chitosan-CNTs	Phenol	1 g/L, 45 °C, 3 h, pH 5, 50 – 300 mg/L	86.96	Langmuir	PSO	(Guo et al., 2019)
Chitosan	Phenol	1 g/L, 45 °C, 3 h, pH 5, 50 – 300 mg/L	61.69	Langmuir	PSO	
Chitosan-GO (M)	Tetracycline	0.05 g/L, 40 °C, 3 h, pH 10, 20 – 200 mg/L	500.68	Langmuir	PSO	(Liu, Liu et al., 2019)
Chitosan-GO (M)	Ciprofloxacin	0.33 g/L, rT °C, 8 h, pH 5, 2 – 100 mg/L	282.9	Langmuir, Freundlich	PSO	(Wang, Yang et al., 2016)
Chitosan-GO (M)	Ibuprofen	0.05 g/L, 35 °C, 3 h, pH 6, 1 – 10 mg/L	160.38	Langmuir	PSO	(Liu, Liu et al., 2019)
Chitosan-GO (M)	Tetracycline	0.4 g/L, 25 °C, 8 h, pH 6, 0 – 0.2 mM	110.0	Langmuir, Freundlich	PSO	(Huang et al., 2017)
Chitin-GO	Ciprofloxacin	5 g/L, 25 °C, pH 6.3, 4 – 850 mg/L	73.0	Sips		(González et al., 2018)
Chitosan-GO (M)	Monuron	0.2 g/L, 25 °C, 0.67 h, pH 5, 1 – 20 μg/mL	35.72	Langmuir	PSO	(Shah et al., 2018)
Chitosan-GO (M)	Isoproturon	0.2 g/L, 25 °C, 0.67 h, pH 5, 1 – 20 μg/mL	33.33	Langmuir	PSO	(Shah et al., 2018)
Chitosan-GO (M)	Linuron	0.2 g/L, 25 °C, 0.67 h, pH 5, 1 – 20 μg/mL	29.41	Langmuir	PSO	(Shah et al., 2018)

AC: activated carbon, C: carbon; BC: biochar, CNTs: carbon nanotubes, GO: graphene oxide, G: graphene, M: magnetic, q_{max}: maximum uptake.

Analysis of cadmium Cd^{2+} adsorption on chitosan-biochar composite showed that both Langmuir and Freundlich models presented high R^2 of 1.0 relative to R^2 of 0.753 for Dubinin-Radushkevich model (Zhang, Tang et al., 2019). This confirmed the existence of both mono and multilayers adsorption (Mallakpour & Khadem, 2019). Langmuir model exhibited a maximum capacity q_{max} of 370.37 mg/g for Cd^{2+} on CS-BC. The PSO model showed best analysis for the adsorption kinetic data with R^2 of 1.0 compared to 0.621 for PFO. These results suggested a chemisorption phenomenon involving the interchange of electrons between Cd^{2+} ions and CS-BC (Fan, Luo, Sun, Li et al., 2013). Moreover, the intra-particle diffusion linear plot showed three slopes which confirmed the existence of more than one rate-determining step (Zhang, Luo et al., 2016). The adsorbed amount of Cd^{2+} increased from 66 to 74 mg/g within the pH range of 2–3 and remained without change at pH > 3. The electrostatic repulsion between positive CS-BC surface and positive charge ions was decreased the attraction of Cd^{2+} at low pH value (Rahmi & Nurfatimah, 2018). The kinetic data showed that > 90% of the equilibrium-adsorbed Cd^{2+} could be removed within 1 h and the saturation was attained at 3 h. This result indicated rapid attraction of Cd^{2+} by CS-BC which could be related to the availability of active sites on CS-BC. Xiao et al. (2019) showed that magnetic CS-BC composite exhibited adsorption capacities towards Cr (VI) and Cu(II) of 26% and 18% higher than those of the original CS-BC composite. This could be attributed to the existence of various mechanisms for the interaction between magnetic CS-BC and Cr(VI)/Cu(II) which included physical adsorption and precipitation, surface complexation and ion exchange.

The best analysis of Langmuir and PSO models was also observed for the chromium adsorption on magnetic chitosan-carbon nanotubes (CS-CNTs) composite (Neto et al., 2019). The Langmuir equation showed proper fitting with $R^2 > 0.990$ for Cr(III) and Cr(VI) adsorption relative to R^2 (0.860 − 0.980) for Freundlich model. The q_{max} values of Cr(III) were 66.25 and 73.30 mg/g; and of Cr(VI) were 449.30 and 477.30 mg/g at 25 °C and 40 °C, respectively. This indicated that attraction of both metal ions on the magnetic CS-CNTs was endothermic and R_L values (0.034 − 0.201) confirmed the favorable adsorption (Subedi et al., 2019). The PSO equation exhibited well kinetic analysis for two metals with $R^2 > 0.981$. Meanwhile, the PFO model exhibited R^2 within the range (0.534 − 0.971). This suggested that the system of Cr(III)/Cr(VI) and magnetic CS-CNTs showed a PSO kinetic and the rate-limiting step was chemical adsorption (Zhang, Tang et al., 2019). The linear plot of intra-particle diffusion equation exhibited two slopes which indicated that adsorptive process was affected by multiple steps (Luo, Fan, Xiao, Sun, & Zhou, 2019; Subedi et al., 2019). The saturation states were achieved in 150 min and 60 min for Cr(III) and Cr(VI), respectively. Removal of Cr(III) was enhanced from 5 to 70% in the pH range from 2.0 to 8.0, and then decreased to 52% at pH 10.0 due to formation of Cr $(OH)_3$ precipitate. The largest percentage of Cr(VI) removal (97%) was obtained within the pH range from 4.0 to 5.0. The pH value of magnetic CS-CNTs composite at the point of zero charge (pH_{PZC}) was 5.6. Therefore, the surface of magnetic CS-CNTs at pH < pH_{PZC} would be positively charged which favored interaction with the Cr(VI) anions (Anush, Chandan, & Vishalakshi, 2019; Xiao et al., 2019). However, at pH > pH_{PZC} the existence of negative charges reduced the attraction of anionic Cr(VI) species towards the negatively charged surface of magnetic CS-CNTs composite.

Adsorption behavior of lead Pb(II) on magnetic chitosan/graphene oxide (CS-GO) composite was performed under various conditions and analyzed by different models (Samuel et al., 2018). The experimental isotherm data was well fitted by Langmuir isotherm (R^2 = 0.962 − 0.993) compared to Freundlich model (R^2 = 0.951 − 0.979). This revealed the uniform distribution of active sites on the magnetic CS-GO composite surface (Luo et al., 2019). Hence, Pb(II) adsorption followed the monolayer coverage. In comparison to the PFO (R^2 = 0.681 − 0.874) and intra-particle diffusion (R^2 = 0.880 − 0.959) models, the PSO model was a best fit (R^2 = 0.987 − 0.998). This model suggested the proportionality of the rate of adsorption to the difference between adsorbed amounts at saturation and at specified time (Hu et al., 2018). According to PSO model, the $q_{e,cal}$ values were increased from 24.64 to 65.79 mg/g with enhancing inlet Pb(II) amount from 25 to 100 mg/L. The high amount of Pb(II) ions in inlet solution enhanced the transfer of these ions towards adsorbent (Dou et al., 2019). The results also showed that the pore diffusion was not the rate-determining step. When pH value increased from 2.0 to 5.0, the Pb(II) adsorption greatly enhanced from 3% to 90%. This could be ascribed to to the abundance of structural groups like $–COO^-$ and $–O^-$ which could react with Pb(II) ions to form complex and thereby enhanced adsorption (Li et al., 2015). The decline in adsorption at low pH was related to the protonation of these groups which induced an electrostatic repulsion of Pb(II) ions (Fan, Luo, Sun, Li et al., 2013). The adsorption efficiencies of Pb(II) ions were 65% and 92% at 20 °C and 27 °C.

The literature also included the adsorption of Ni(II) and Zn(II) on chitosan-biochar composite (Zhang, Tang et al., 2019). The adsorption data were best analyzed by the Langmuir and PSO equations which confirmed the monolayer and chemisorption natures. The values of q_{max} were 114.94 and 99.01 mg/g for both metals, respectively. The adsorption of As(V) on chitosan-graphene oxide composite (Kumar & Jiang, 2016) and Hg(II) on chitosan-graphene composite (Zhang et al., 2014) were also included. The values of q_{max} were 71.90 and 361.0 mg/g for As(V) and Hg(II), respectively. For As(V), Freundlich model well analyzed the isotherm data, meanwhile for Hg(II) the Langmuir model was the best. PSO kinetic model exhibited well representation for kinetic data of both adsorption systems.

Langmuir model well correlates the isotherm data of most metal ions on chitosan/chitin-carbonaceous material composites. Freundlich model with or without Langmuir model is also applicable in some cases. From the parameters of both models the adsorption process is favorable. PSO kinetic model shows best representation for kinetics data. Table 2 shows that the most widely used carbonaceous materials are graphene oxide and activated carbon followed by carbon nanotubes, biochar and graphene. Moreover, the most widely utilized biopolymer is chitosan and the most studied metals are copper, chromium, cadmium and lead. Incorporation of carbonaceous materials to chitosan/chitin enhances the adsorption performance towards metal ions. In this context, chitosan-GO composite exhibits adsorption capacity toward Cu (II) of about 10 times more than that of chitosan alone. Also, the adsorbed amount of Cd(II) on AC-chitosan composite is about 5 times more than that of Cd(II) on chitosan (Table 2). This confirms the role of high surface areas GO and AC carbonaceous materials in development of chitosan structure and enhancement of chitosan performance towards heavy metals removal. Moreover, the magnetic composites show high adsorption performance towards metal ions as compared to original composite. This can be due to the role of magnetic iron materials in development of porous structure of original composite structure and improvement of its functional groups.

4.2. Synthetic dyes

Dyes are common organic pollutants owing to their widely utilization and production (Han et al., 2019). Most of dye molecules have complex and non-degradable natures; hence they can decrease the transmission of sunlight into the water and affects the aquatic systems. Moreover, dyes act as toxic materials towards humans and other organisms (Wong et al., 2018). Dyes are normally categorized into (i) anionic (acid, direct and reactive dyes), (ii) cationic (basic dyes) and (iii) non-ionic (dispersed dyes) (Yagub, Sen, Afroze, & Ang, 2014). Synthetic dyes are mostly dissolved in water with a little are dispersive. Methylene blue (MB), malachite green (MG) and crystal violet (CV) are examples of common cationic dyes. Meanwhile, methyl orange and congo red (CR) are common anionic dyes (Lai, Lee, Hiew, Thangalazhy-Gopakumar, & Gan, 2019). According to the data (Table 3), the most studied dye is methylene blue due to its sever toxicity and high coloring influences on aquatic systems (Han et al., 2019). MB can affect skin, eye

and brain (Wong et al., 2018). MG is extremely noxious to organs such as kidney, liver, spleen, lung and eyes. Consumption of the CV dye causes various health problems such as tissue necrosis, skin irritation, jaundice and vomiting. MO is mutagenic and carcinogenic substance against organisms. CR can cause mutation in DNA of organisms in ecosystems (Daud et al., 2019). Therefore, several studies were addressed the removal of these dyes by using chitosan/chitin-based composites.

Karaer and Kaya (2016) tested the methylene blue adsorption on magnetic chitosan-activated carbon (CS-AC) composite. Langmuir model exhibited better analysis for isotherm data with the highest average R^2 of 0.970 as compared to average R^2 of 0.766 for the Freundlich model. This confirmed the evenly distribution of MB over homogeneous magnetic CS-AC surface. Similar result was observed for MB adsorption on chitin-GO composite (Ma et al., 2016). The maximum reported uptakes q_{max} of MB were 200, 333, and 500 mg/g at 25 °C, 35 °C, and 45 °C, respectively, based on the Langmuir equation. This revealed the endothermic nature for MB adsorption on composite (Auta & Hameed, 2013). The values of Freundlich parameter n (1.09–2.82) were greater than one which indicated the favorable MB/CS-AC system (Zhang et al., 2018). The kinetic data of the MB/CS-AC system were best analyzed by the PSO equation with R^2 (0.962 − 0.981) relative to R^2 (0.793 − 0.893) for PFO equation. This indicated the high dependence of the adsorption process on chemisorption which involved the interaction between C—O—C groups and ammonium cation of MB. The equilibrium state was achieved within the period of 200 − 300 min. The uptake of MB enhanced from 12.5 to 166.5 mg/g as the inlet MB amount was enhanced from 50 mg/L to 500 mg/L. This could result from the presence of more MB molecules which enhanced their transfer towards adsorbent (Lai, Hiew et al., 2019). Also, it was observed that the highest adsorption of MB was reported at pH 11. The high adsorption was under alkaline conditions because of the electrostatic attraction between cationic MB dye and negatively charged CS-AC surface and under acidic conditions, H^+ ions prevented such attraction (Yan, Huang, & Li, 2019). The effects of initial dye concentration, pH and temperature on adsorption capacity showed that the initial concentration of the dye was strongly affected the adsorption performance compared to other adsorption factors. The adsorption mechanism showed that the intra-particle diffusion is not the rate limiting step.

Adsorption of cationic crystal violet dye was studied on chitosan based adsorbent in terms of chitosan-activated carbon composite (Kumari, Krishnamoorthy, Arumugam, Radhakrishnan, & Vasudevan, 2017) Based on R^2 values (0.991 − 0.999) for the Langmuir relative to (0.914 − 0.996) for the Freundlich, the former equation provided the well correlation of the data which implied monolayer adsorption system (Debnath, Parashar, & Pillay, 2017). The q_{max} values decreased from 12.5 mg/g at 40 °C to 1.77 mg/g at 60 °C which revealed exothermic adsorption. This could be due to decrease in bonding strength between the dye and active sites of the composite (Karaer & Kaya, 2016). From the kinetic analysis, the R^2 values remained below 0.965 for the PFO model. However, the PSO model showed R^2 values above 0.987. Therefore, the PSO equation best represented the CV attraction on the composite which suggested chemisorption rate-controlling step (Zhu et al., 2010). The equilibrium was achieved after 40 min and the enhancement in initial CV concentration favored adsorption due to intense concentration gradient and high driving force (Ma et al., 2016). At pH 9, high adsorption (99%) was reported due to the electrostatic attraction of cationic CV dye towards negatively charged composite (Gul et al., 2016). The increasing in composite amount from 0.2 to 0.4 g enhanced adsorption, and then insignificantly decreased which might be related to the decrease in active sites caused by the aggregation. The adsorption mechanism showed that the pore diffusion was not only the rate-limiting step but also some unpredicted mechanism included in the process. Arumugam, Krishnamoorthy, Rajagopalan, Nanthini, and Vasudevan (2019) also showed monolayer coverage, chemisorption, exothermic and spontaneous behavior for adsorption of cationic malachite green dye on chitosan-activated carbon composite.

The analysis of isotherm data of anionic congo red adsorption on chitosan-carbon nanotubes composite showed R^2 and chi-square χ^2 values of (0.998, 10.41), (0.905, 113.46) and (0.998, 4.22) for the Sips, Freundlich, and Langmuir equations, respectively (Chatterjee, Lee, & Woo, 2010). Therefore, the Langmuir equation exhibited well analysis for the CR/CS-CNTs system. The value of q_{max} from this equation was 450.4 mg/g. The R_L value (0.031) computed at the inlet CR amount of 1000 mg/L revealed preferable attraction of CR onto the CS-CNTs (Li et al., 2014). The parameter n (0.98) of the Sips model indicated a uniform adsorption (González et al., 2015). The R^2 value of the PFO equation was 0.994 and the R^2 value of the PSO was 0.977, revealing best analysis of kinetic data by PFO equation (Debnath et al., 2017; Lai, Hiew et al., 2019). The high R^2 value suggested an important role for the pore diffusion in the initial adsorption of CR onto the CS-CNTs composite. The saturation was attained at 360 min with the highest uptake of 400 mg/g. For the initial CR amount of 500 mg/L and pH 5, the uptakes of CS-CNTs and CS were 400 and 350 mg/g, respectively. This might be as a result of the large surface area of CS-CNTs as compared to that for CS alone. The CR/ CS-CNTs system was greatly pH dependent and highest uptake of 423.1 mg/g attainted at pH 4. Within the pH range of 4–9, the uptake of CR decreased from 423.1 to 253.2 mg/g. This could be due to the presence of high content of NH_2 groups in CS-CNTs structure which favored attraction of anionic CR dye at low pH value.

Jiang et al. (2016) examined the performance of magnetic chitosan-graphene oxide (CS-GO) composite adsorbent for methyl orange dye. The Langmuir model well represented the data with the better R^2 (0.9897) than Freundlich model (R^2 = 0.9112), which suggested a uniform surface with identical sites activity (Banerjee, Barman, Mukhopadhayay, & Das, 2017). The high surface area of GO and high functionality of CS exhibited CS-GO of a higher performance (q_{max} = 398.08 mg/g) to MO. This value was higher than 230.91 mg/g that reported for MO on chitosan-graphene composite (Zhang et al., 2018). The value of R_L (0.0929) was between 0 and 1 which indicated a favorable MO/CS-GO system. The PSO model presented good analysis for the kinetics (R^2 = 0.9763) than the analysis of PFO model (R^2 = 0.9653). For the MO sample of 50 mg/l, high uptake of 50.98 mg/g was achieved at 60 min followed by slight fluctuation until attainment of saturation at about 180 min. The initial high uptake of dye could be due to the abundance of active sites on CS-GO (Marrakchi, Ahmed, Khanday, Asif, & Hameed, 2017). The MO uptake by CS-GO slightly reduced by changing the pH from 4 to 10 and the largest adsorbed amount (55 mg/g) was found at an initial pH 4 and the pH_{PZC} value of CS-GO was about 10. At lower pH, the positively charged CS-GO exhibited a favorable electrostatic attraction toward anionic MO dye (Zhu et al., 2010). The uptake percentage enhanced from 56.0% to 88.4% with changing composite dosage from 0.25 to 2 g/L. Meanwhile, the uptake decreased from 98 to 20 mg/g with the same change in dosage. The presence of more composite dosage provided more active sites which might lead to a weak occupation of site at a specific dye amount (Yan et al., 2019). The analysis of factors was confirmed that inlet dye amount and CS-GO dosage exhibited high significant influence on uptake relative to the initial pH.

The removal of other dyes on chitin/chitosan-carbonaceous material composites was also studied (Table 3). Magnetic chitosan-AC and chitosan-AC composites exhibited q_{max} of 250.0 and 596.4 mg/g for reactive blue 4 (Karaer & Kaya, 2016) and acid blue 29 (Auta & Hameed, 2013), respectively. The studied systems followed the Langmuir and PSO equations. Rose bengal (Abdel Salam et al., 2014) and direct blue 7 (Abbasi & Habibi, 2016) were adsorbed on magnetic chitin-CNTs and chitosan-CNTs composites with q_{max} of 6.25 and 29.33 mg/g. Adsorption data of remazol black and neutral red on chitin-GO composites (González et al., 2015) were well fitted by Sips and PFO models. High uptake of 1085.3 mg/g was observed for rhodamine B on magnetic chitosan-GO (Marnani & Shahbazi, 2019).

Freundlich model was well analyzed the adsorption data of acid red on chitosan-G composite with q_{max} of 132.94 (Zhang et al., 2018).

Langmuir model is most appropriate for analysis of the isotherm data of most dyes on chitosan/chitin-carbonaceous material composites. Freundlich model with or without Langmuir model is also applicable in some cases. The parameters in both models confirm that the adsorption process is favorable. PSO kinetic model exhibits good analysis for the kinetics data with applicability of PFO in some cases. Table 3 shows that the most widely utilized carbonaceous materials are graphene oxide and activated carbon followed by carbon nanotubes and graphene. In addition, methylene blue is the most widely tested dye and its highest adsorption capacities are 1023.9 and 500.0 mg/g on chitosan-GO and magnetic chitosan-AC composites, respectively. The high adsorption capacity of MB on chitosan-GO composite can be related to the role of electrostatic attraction, hydrogen bonding, and π–π interaction mechanisms in adsorption process. Most of studies include chitosan with few studies about chitin which can be attributed to the limited solubility of chitin as compared to chitosan. Moreover, chitosan-GO composite shows higher adsorption towards MB dye than chitin-GO composite. The reason behind that is the existence of free amino groups in chitosan structure which are more active than the acetamide groups in chitin structure. Chitosan/chitin-carbonaceous materials composite shows high adsorption capacity towards dyes relative to chitosan alone. For instance, the uptakes of MB on raw chitosan and chitosan-AC composite are 234.5 and 388.1 mg/g, respectively. Also, the adsorption capacities of chitin and chitin-GO composite adsorbents towards neutral red are 17.04 and 165.0 mg/g, respectively.

4.3. Other pollutants

In addition to the heavy metals and dyes, adsorption of other contaminates such as pharmaceuticals, phenols, herbicides, nitrate and phosphate is also presented (Table 4). The majority of published studies were about pharmaceuticals due to their extensive consumption by humans and animals, continuous release by hospitals and medicine factories, stability and negative effect on the environment (Ahmed & Hameed, 2018). The most tested drugs are ciprofloxacin and tetracycline antibiotics which are widely used to treat bacterial infections. In addition, the presence of these antibiotics in water can produce resistant bacteria, which poses a potential threat to human and animal health (Wu et al., 2019). Amoxicillin, cephalexin and erythromycin along with ibuprofen (non-steroidal anti-inflammatory drug) are also considered. Phenolic pollutants are found in different industrial wastewaters such as petrochemical, plastics, insecticide, leathers, resins, etc. The existence of these pollutants in water, even at low amounts, can affect aquatic organisms. They also cause human diseases such as cancer, jaundice, skin disease and even death (Hejazi, Ghoreyshi, & Rahimnejad, 2019). Phenylurea herbicides such as monuron, linuron and isoproturon are utilized for weed control which affects negatively the agricultural crops production. The acceptable limit for a herbicide in drinking water is 100 ng/L. These herbicides are toxic and can lead to cancer (Shah, Jan, & Tasmia, 2018). The presence of nitrate and phosphate in water causes excessive growth of aquatic plants and organism. Consequently, decreases the oxygen content of water which has a negative impact on aquatic life as a result of a phenomenon called eutrophication. The acceptable levels of nitrate and phosphate in drinking water are 40 and 0.1 mg/L, respectively (Karthikeyan & Meenakshi, 2019). Thus, these pollutants have been extensively treated by using chitosan/chitin-based composites.

Wang, Yang et al. (2016) tested the ciprofloxacin adsorption on magnetic chitosan-graphene oxide composite. Langmuir and Freundlich equations (R^2 = 0.995 and 0.992) were best correlated the isotherm data which suggested complex adsorption of CIP on CS-GO with q_{max} of 282.9 mg/g. The reported q_{max} values of CIP on magnetic chitosan-activated carbon (Danalıoğlu et al., 2017) and chitosan-biochar (Afzal et al., 2018) composites were 90.10 mg/g and 78.79 mg/g, respectively. Thus, chitosan–graphene oxide composite exhibited high adsorption performance toward ciprofloxacin as compared to chitosan-activated carbon and chitosan-biochar composites. This could be related to the efficient attraction between negative structural groups on CS-GO and cationic CIP species. Moreover, the q_{max} of CIP on chitin-GO composite was reported as 73.0 mg/g (González et al., 2018). This confirmed the high adsorption performance of chitosan-GO as compared to chitin-GO composite which could be related to the presence of active free amino groups in the chitosan structure. About 66% enhancement in adsorption capacity of chitosan towards CIP was reported by incorporation of GO to chitosan structure. The magnitude of Freundlich parameter (n = 1.341) was < 1 which indicated a preferable adsorption system (Khanday et al., 2019). The R^2 for PSO model was 0.998 relative to 0.950 for PFO. This confirmed the best analysis of PSO and suggested chemisorption nature (Huang et al., 2017). The uptake rate of CIP was initially rapid during the 2 h then declined until attained saturation (~8 h). Increasing pH from 4 to 5 enhanced the q_e from 33.75 to 35.25 mg/g then reduced to 23.75 mg/g at pH 7. Within pH range of 4.0–5.0, the uptake of CIP declined only 4.7%. The drop in CIP uptake at pH of 7.0 might result from greatly depressed attraction between hydrophobic CIP and the hydrophilic CS-GO (Li et al., 2014).

Analysis of isotherm data of the tetracycline adsorption on $FeSO_4$ modified chitosan-biochar (FeCS-BC) composite showed that the Sips equation exhibited the largest R^2 (0.977–0.998) compared to R^2 (0.961–0.995) for Langmuir equation and R^2 (0.846–0.915) for Freundlich model (Liu, Zhou et al., 2019). Sips equation includes both Freundlich and Langmuir formulas. The best analysis of Sips equation was also observed for the system of antibiotics on chitin-GO composite (González et al., 2018). The magnitudes of n (0.869–1.3863) slightly deviated from 1, indicating the existence of some heterogeneity despite the homogeneous structure of FeCS-BC. According to the Sips model, the value of q_{max} was increased from 176.24 to 252.78 mg/g with changing temperature from 25 °C to 45 °C. The value of 252.78 mg/g is lower than 500.68 mg/g reported for tetracycline on chitosan-graphene oxide composite (Liu, Liu, Li, Yu, & He, 2019). The results also showed the favorable role of $FeSO_4$ in enhancement of adsorption performance of FeCS-BC composite. Increasing the amount of $FeSO_4$ from 1 to 1.7 g resulted in about 48% enhancement (86.7–128.0 mg/g) in adsorption performance of biochar-chitosan composite towards tetracycline antibiotic. This could be ascribed to the effects of ion exchange, chelating, and hydrogen bonding. The existence of Fe-O group in $FeSO_4$ modified composite improved its attraction for tetracycline by chelating mechanism. PSO equation well fitted the data of TC adsorption on FeCS-BC due to larger R^2 (0.971 − 0.978) relative to R^2 (0.915 − 0.935) for PFO equation. More than 80% of TC removal was achieved at 4 h followed by the saturation state at about 12 h. The influence of pH (2–12) presented that the highest adsorbed amount was obtained as 180.39 mg/g at pH 5. The pH_{PZC} of FeCS-BC was reported as 5.16. The lower adsorption of TC at pH < 5 and pH < 5 resulted from the repulsive force between the similar charges of TC species and composite. At pH 5, the strong π-π contact could occur between π on composite surface and benzene ring in TC molecules (Huang et al., 2017). The adsorption mechanism showed the participation of pore and film diffusion steps in adsorption. Thermodynamic results suggested that TC adsorption was endothermic, spontaneous and controlled by the physis-chemisorption step.

Adsorption of other antibiotics such as amoxicillin and erythromycin was also tested using magnetic chitosan-activated carbon composite (Danalıoğlu et al., 2017). Langmuir equation presented better fitting for the isotherm data of both drugs with R^2 (0.926 − 0.929) relative to R^2 (0.391 − 0.793) for Freundlich model. This confirmed the monolayer coverage on homogeneous surface. The values of q_{max} of amoxicillin and erythromycin were 526.31 and 178.57 mg/g, respectively. Adsorption kinetic data of amoxicillin and erythromycin on magnetic CS-AC best fitted with PSO kinetic model with R^2 (0.934 − 0.998) relative to R^2 (0.507 − 0.852) for PFO model.

The adsorption was taken place rapidly for both of the adsorbates at the first 30 min. Then, the uptake rate became slower, and after 120 min, the system reached the equilibrium state. The best application of Langmuir model and PSO kinetic model was also reported for ibuprofen adsorption on magnetic chitosan-graphene oxide composite (Liu, Liu et al., 2019). According to the Langmuir equation, the value of q_{max} was 160.83 mg/g at 35 °C. The influence of contact time on the attraction of ibuprofen on magnetic CS-GO was significantly enhanced the uptake rate within 120 min and continued without changing. The uptake was improved from 19.92 to 150.28 mg/g when the inlet ibuprofen amounts changed by 1–10 mg/L. The uptake of ibuprofen was also enhanced from 81 to 122 at pH 2–6 and decreased to 66 mg/g at pH 12. The decrease in uptake rate could be caused by the electrostatic repulsion (Huang et al., 2017).

Adsorption behavior of phenol was tested on chitosan-based adsorbent in terms of chitosan-carbon nanotubes CS-CNTs composite (Guo et al., 2019). The R^2 values of Freundlich and Langmuir equations were 0.981 and 0.997, respectively. Thus, the Langmuir equation accurately described the adsorption of phenol which confirmed single-layer adsorption of phenol on composite (Khakpour & Tahermansouri, 2018). According to the Langmuir model, the q_{max} at 45 °C was enhanced from 61.69 to 86.96 mg/g for original chitosan and chitosan-carbon nanotubes composite, respectively. This demonstrated the role of carbon nanotubes in enhancement of chitosan performance. The value of $1/n < 1$ confirmed a preferable process. In addition, the $1/n$ magnitudes of CS-CNTs and CS were 0.49 and 0.62 which indicated the more easily attraction of phenol on composite than chitosan alone. The PSO equation showed the well analysis of phenol data ($R^2 = 0.97$), followed by the PFO and Elovich equations. This showed that the PSO model was well represented the phenol attraction on CS-CNTs (Alves et al., 2019), and revealed the chemisorption nature. The equilibrium time was 24 h with an uptake of 50.76 mg/g. Phenol uptake on CS-CNTs increased from 22.5 to 66.4 mg/g with changing temperature from 35 to 45 °C which confirmed endothermic nature. The uptake of CS-CNTs composite increased from 23.5 to a maximum of 39.4 mg/g as the pH changed from pH 3–5, and the decreased to 27.5 mg/g at pH of 9. The decrease in uptake under basic media could be due to the hydrogen bonding between OH ions of CNTs and water which reduced the active sites of the CS-CNTs adsorbent. As the phenol amount enhanced from 50 to 300 mg/L, the equilibrium uptake was also increased from 17.5 to 68 mg/g as a result of the enhanced driving force. These driving forces weakened all the resistances of phenol transfer from the bulk solution to adsorbent which caused a better attraction of phenol on the active sites (Soni, Bajpai, Singh, & Bajpai, 2017).

Similar adsorption behavior was reported for phenylurea herbicides including monuron, isoproturon and linuron on magnetic chitosan graphene oxide composite (Shah et al., 2018). The Langmuir equation ($R^2 = 0.997 - 0.998$) gave a well analysis than Freundlich equation ($R^2 = 0.934 - 0.978$) as confirmed by the large R^2. This suggested the monolayer coverage (Danalıoğlu et al., 2017). The q_{max} values were 35.72, 29.41, and 33.33 mg/g for monuron, isoproturon, and linuron, respectively. The magnitudes of ($n = 2.247$–2.564) were higher than 1 for all the adsorbates which indicated the preferable attraction process (Khanday et al., 2019). The high values of R^2 ($0.994 - 0.998$) showed that the attraction of these adsorbates on the magnetic GO-CS composite followed PSO equation relative to PFO equation ($R^2 = 0.889 - 0.916$). The effect of contact time showed rapid kinetic with achieving of saturation beyond 40 min. This could be due to the initial abundance of vacant sits which then reduced due to their occupation by adsorbates (Marrakchi et al., 2017). The results revealed that the highest uptake of adsorbates obtained at pH 5.0. Low adsorption at pH < 5 was caused by the repulsion between positive composite surface and protonated nitrogen groups of the adsorbates. The uptake was also reduced at pH < 5 because of the negative composite surface and the presence of adsorbates in non-ionic states. The adsorption of herbicides was improved by using more composite dosages as a result of the abundance of more sites for the interaction between herbicide and the composite (Jiang et al., 2016). The C values of intra-particle diffusion model were greater than zero (5.198–14.930) which confirmed the complex adsorption including physisorption and chemisorption.

Banu, Karthikeyan, and Meenakshi (2019) tested the nitrate and phosphate adsorption on chitosan-activated carbon composite. The greater R^2 (< 0.99) and smaller χ^2 (0.121) indicated more suitability of Freundlich than Dubinin–Radushkevich (D–R) and Langmuir equations. The magnitudes of $1/n$ ($0.654 - 0.851$) were less than 1 indicated a favorable process (Abbasi & Habibi, 2016). The K_F magnitude enhanced with increase in heating for both phosphate and nitrate which revealed endothermic behavior. The E magnitudes of the D–R equation were more than 8 kJ/mol further indicated the chemisorption process (Afzal et al., 2018). The q_{max} values were 90.09, 103.39, and 124.57 mg/g for nitrate adsorption and 131.29, 146.06, and 154.72 mg/g for phosphate adsorption at 30 °C, 40 °C, and 50 °C, respectively. The R^2 of the PSO model was higher than 0.99 for both adsorbates at 30 °C which confirmed more accurate representation of kinetic data by PSO than PFO equation (Alves et al., 2019). The $q_{e,cal}$ values were increased from 38.68 to 77.75 mg/g for nitrate and from 46.18 to 95.36 mg/g for phosphate with enhancing inlet amount from 100 to 200 mg/L. Moreover, the k_2 magnitudes were enhanced from 0.022 to 0.029 g. mg/min for nitrate and from 0.022 to 0.025 g. mg/min for phosphate within the same increase in initial concentration. The uptakes of phosphate and nitrate enhanced with increasing of inlet concentration due to the transfer of more ions towards the active sites of composite (Khanday et al., 2019). The increase of composite dosages from 0.025 to 0.15 g enhanced removal of phosphate from 41 to 98% and nitrate from 35 to 85%. At high composite dosages, the number of active sites enhanced which resulted in attraction of more ions on the composite (Shah et al., 2018). The uptake of nitrate enhanced within pH 3–7 and it enhanced till pH 8 for phosphate. However, lower adsorption was reported under more alkaline medium which might be related to the high competitive effect and diffusion impeding of OH ions. Cui et al. (2019) showed that the $FeCl_3$ modified CS-carbon composite exhibited removal efficiencies towards nitrate and phosphate of 90.6% and 97.4% relative to 36.4% and 67.7% for raw CS-carbon composite, respectively. This suggested that the doping of $FeCl_3$ greatly improved the sorption capacity. The electrostatic attraction, hydrogen bonding and ion exchange induced by the graft of $FeCl_3$ were the potential mechanisms for nitrate and phosphate sorption onto $FeCl_3$ modified composite.

Langmuir model exhibits well-fitting pattern for the isotherm data of most pollutants on chitosan/chitin-based composites. Freundlich model with or without Langmuir model is also applicable in some examples and the parameters of both models reveal favorable adsorption processes. PSO model shows best representation for kinetics data with applicability of PFO in some cases. Table 4 shows that the most widely explored pollutants are antibiotics, particularly ciprofloxacin and tetracycline. Chitosan-GO and chitosan-AC composites show high adsorption capacity towards pharmaceutical pollutants compared to chitosan-BC composite. In addition, chitosan-GO exhibits high adsorption capacity towards ciprofloxacin compared to chitin-GO composite. Carbonaceous materials have a significant role in enhancement of chitosan performance toward pollutants. For instance, the adsorption capacity of phenol on chitosan-CNTs composite is 86.96 mg/g relative to 61.69 mg/g on raw chitosan (Table 4). Moreover, magnetic composites show enhanced adsorption towards pollutants than the original composites. This confirms the more developed structure of magnetic composite adsorbent either by improvement of pore properties or enrichment of active functional groups.

5. Regeneration and reusability of adsorbents

The successive regeneration and reuse of adsorbents are significant criteria for their practical applications. The potential adsorbent should exhibit an efficient regeneration and great capability to be reutilized

Table 5
Regeneration performances of various chitosan/chitin-based composites loaded with heavy metals, synthetic dyes, and other pollutants.

Adsorbent	Pollutant	Eluent	Adsorption; desorption conditions	No. of cycles	Change in capacity or removal (%)	Reference
Chitosan-BC (M)	Cu(II)	NaOH	0.5 g/L, 30 °C, 24 h, pH 7, 40 mg/L; 0.1 M NaOH, 50 mL, 2 h	3	51.13 – 42.6 mg/g	(Xiao et al., 2019)
Chitosan-BC (M)	Cr(VI)	NaOH	0.5 g/L, 30 °C, 24 h, pH 3, 40 mg/L; 0.1 M NaOH, 50 mL, 2 h	3	30.06 – 23.34 mg/g	(Xiao et al., 2019)
Chitosan-BC	Ciprofloxacin	NaOH	5 g/L, 30 °C, 24 h, pH 3, 50 mg/L; 1 N NaOH, 200 mL, 0.5 h, 250 rpm	6	32.5 – 25.5 mg/g	(Afzal et al., 2018)
Chitosan-CNTs (M)	Cr(III)	NaOH	0.3 g/L, 25 °C, 3 h, pH 4, 100 mg/L; 0.1 M NaOH, 10 mL, 3 h	10	26 – 14%	(Neto et al., 2019)
Chitosan-CNTs (M)	Cr(VI)	NaOH	0.3 g/L, 25 °C, 3 h, pH 4, 100 mg/L; 0.1 M NaOH, 10 mL, 3 h	10	98 – 93%	(Neto et al., 2019)
Chitosan-CNTs (M)	Pb(II)	NaOH	0.4 g/L, 25 °C, 2 h, pH 5, 50 mg/L; 0.1 M NaOH, 10 mL, 3 h	5	81.25 – 72.5%	(Wang et al., 2015)
Chitosan-CNTs	Cr(VI)	NaOH	1 g/L, 30 °C, 2 h, pH 2, 200 mg/L; 0.1 M NaOH, 50 mL, 30 °C, 2 h	5	100–91%	(Huang et al., 2018)
Chitosan-CNTs	Tri-nitrophenol	NaOH	0.29 g/L, 25 °C, 5 h, pH 7, 100 mg/L; 1 M NaOH, 70 mL, 25 °C, 5 h	5	91 – 79.7%	(Khakpour & Tahermansouri, 2018)
Chitosan-GO (M)	Cr(VI)	NaOH	1 g/L, 25 °C, 1.5 h, pH 2, 50 mg/L; 1 M NaOH, 25 mL, 25 °C, 2 h, 180 rpm	7	92.5 – 87.5% 46 – 44 mg/g	(Zhang, Luo et al., 2016)
Chitosan-GO (M)	Cr(VI)	NaOH	0.5 g/L, 22 °C, 4 h, pH 2, 40 mg/L; 0.1 M NaOH	4	77.5 – 75%	(Subedi et al., 2019)
Chitosan-GO	As(V)	NaOH	8 g/L, 30 °C, 1 h, pH 5.4, 150 rpm; 1 M NaOH, 10 mL	5	99 – 82.5%	(Kumar & Jiang, 2016)
Chitosan-GO (M)	Tetracycline	NaOH	0.4 g/L, 25 °C, 24 h, pH 6, 0.1 mM; 0.05 M NaOH	5	67 – 55 mmol/kg	(Huang et al., 2017)
Chitosan-GO (M)	Tetracycline	NaOH	0.05 g/L, 25 °C, 1.3 h, pH 10; 0.1 M NaOH, 25 °C, 2 h	5	437.2 – 421.2 mg/g	(Liu, Zhou et al., 2019)
Chitosan-GO (M)	Ibuprofen	NaOH	0.05 g/L, 25 °C, 1.3 h, pH 6; 0.1 M NaOH, 25 °C, 2 h	5	113.2 – 96.2 mg/g	(Liu, Liu et al., 2019)
Chitosan-G	Methyl orange	NaOH	16 g/L, °C, 2 h, pH 4, 100 mg/L; 20% NaOH, 25 °C, 12 h, 150 rpm	5	96 – 89%	(Zhang et al., 2018)
Chitosan-AC (M)	Cd(II)	HCl	0.5 g/L, 25 °C, 1 h, pH 6, 100 mg/L; 1 M HCl, 5 mL, 24 h	3	243.1 – 177.7 mg/g	(Sharififard et al., 2018)
Chitosan-GO (M)	Pb(II)	HCl	1 g/L, 27 °C, 24 h, pH 5, 50 mg/L; 0.1 M HCl, 27 °C, 3 h, 120 rpm	4	92 – 78%	(Samuel et al., 2018)
Chitosan-GO (M)	Pb(II)	HCl	0.8 g/L, 30 °C, 1 h, pH 5, 180 rpm; HCl, pH 1	6	90.3 – 75.8%	(Fan, Luo, Sun, Li et al., 2013)
Chitosan-AC	Cd(II)	HNO_3	2 g/L, rT °C, 0.67 h, pH 5, 10 mg/L; 0.001 N HNO_3	4	2.4 – 1.2 mg/g	(Rahmi & Nurfatimah, 2018)
Chitosan-AC (M)	Cd(II)	HNO_3	0.05 g/L, rT °C, 1 min, pH 8, mg/L; 1 M HNO_3, 5 mL	3	95 – 89%	(Yadaei et al., 2018)
Chitosan-GO (M)	Cr(VI)	HNO_3	0.5 g/L, 22 °C, 4 h, pH 2, 40 mg/L; 0.1 M HNO_3	4	70 – 32.5%	(Subedi et al., 2019)
Chitosan-GO (M)	Cu(II)	HNO_3	1 g/L, 20 °C, 1.5 h, pH 5, 80 mg/L; 0.01 M HNO_3	3	95.6 – 88.2%	(Samuel et al., 2018)
Chitosan-GO (M)	Pb(II)	HNO_3	1 g/L, 20 °C, 1.5 h, pH 5, 80 mg/L; 0.01 M HNO_3	3	90.7 – 85.3%	(Samuel et al., 2018)
Chitosan-GO (M)	Cd(II)	HNO_3	1 g/L, 20 °C, 1.5 h, pH 5, 80 mg/L; 0.01 M HNO_3	3	88.4 – 84.6%	(Samuel et al., 2018)
Chitosan-AC	Nitrate	NaCl	2 g/L, 30 °C, 45 min, pH 6.4, 100 mg/L; 0.1 M NaCl, 1 h	5	37.5 – 20 mg/g	(Banu et al., 2019)
Chitosan-AC	Phosphate	NaCl	2 g/L, 30 °C, 30 min, pH 5.3, 100 mg/L; 0.1 M NaCl, 1 h	5	42.5 – 35.5 mg/g	(Banu et al., 2019)
Chitosan-GO (M)	Ciprofloxacin	CH_3OH	0.33 g/L, rT °C, 8 h, pH 5, 20 mg/L; 30 mL CH_3OH	4	94 – 72%	(Wang, Yang et al., 2016)
Chitosan-GO	Methylene blue	EtOH	0.4 g/L, 25 °C, 1.3 h, pH 11, 180 rpm; EtOH, 12 h	5	50 – 32.5 mg/g	(Fan, Luo, Sun, Qiu et al., 2013)
Chitosan-CNTs	Pb(II)	EDTA	1 g/L, 30 °C, 2 h, pH 6, 100 mg/L; 0.1 M EDTA, 24 h	6	83.52 – 72.63 mg/g	(Wang et al., 2020)
Chitosan-G	Cd(II)	EDTA	2 g/L, 25 °C, 5 h, pH 6, 30 mg/L; 0.01 M EDTA, 5 h	3	86 – 80%	(Mallakpour & Khadem, 2019)
Chitosan-BC	Pb(II)	Na_2-EDTA	3.3 g/L, 25 °C, 15 h, pH 6, 400 mg/L; 0.01 M Na_2-EDTA, 50 mL, 100 mg, 25 °C, 15 h	4	100 – 95%	(Zhang, Tang et al., 2019)
Chitosan-AC (M)	Cu(II)	Na_2-EDTA	0.1 g/L, 25 °C, 2 h, pH 5.5, 100 mg/L; 0. 1 M Na_2-EDTA, 2 h	5	100 – 95%	(Li et al., 2017)
Chitosan-GO (M)	Rhodamine	Na_2-EDTA	0.14 g/L, 33 °C, h, pH 7.5, 114 mg/L; 0.1 M Na2-EDTA	7	92.1 – 85.3%	(Marnani & Shahbazi, 2019)
Chitosan-GO (M)	Methyl violet	Acetone	1 g/L, 25 °C, 1 h, pH 10, 10 μg/mL;	4	88 – 83%	(Gul et al., 2016)
Chitosan-GO (M)	Alizarin yellow R	Acetone	1 g/L, 25 °C, 1 h, pH 6, 10 μg/mL;	4	64 – 53%	(Gul et al., 2016)
Chitosan-GO	Methylene blue	HCl + EtOH	0.2 g/L, 30 °C, 24 h, pH 7, 300 mg/L; 1 M HCl-EtOH	5	1005 – 805.1 mg/g	(Yan et al., 2019)
Chitosan-GO	Metanil yellow	NaOH + HCl	0.17 g/L, 30 °C, 1.5 h, pH 6.8, 50 mg/L; 0.1 M NaOH, 1.5 h, 0.1 M HCl, 0.25 h, 30 mL, 5 mg	5	300 – 250 mg/g 98 – 87%	(Lai, Hiew et al., 2019)
Chitin-GO	Methylene blue	NaOH + EtOH	0.4 g/L, 30 °C, 6 h, pH 7, 30 mg/L; 2% NaOH-EtOH mixture (1:1 v/v), 4 h	3	97.1 – 89.5%	(Ma et al., 2016)
Chitosan-G (M)	Methylene blue	EtOH + acetic acid	2.5 g/L, 25 °C, 1.5 h, pH 9, 50 mg/L; 0.5% acetic acid, 50 mL, 2 h, 0.05 g	5	99 – 97%	(Hoa et al., 2016)

AC: activated carbon, BC: biochar, CNTs: carbon nanotubes, GO: graphene oxide, G: graphene, M: magnetic.

many times with the same level of performance (Sherlala et al., 2018). This will offer advantages of minimizing the overall operating cost, recovering of adsorbate molecules and avoiding the formation of solid by-product wastes (Lai, Lee et al., 2019). Many techniques have been adopted for regenerating the adsorbents including chemical, biological and thermal processes. The chemical methods are based on applying suitable agent to desorb or decompose the adsorbates. The advantages of the chemical methods compare to other techniques are relatively rapid process, less energy requirement, no adsorbent loss and the ability to recover the agents and adsorbates (Garba et al., 2019).

A suitable desorbing agent or eluent for regenerating adsorbents should have high activity, low price, eco-friendly nature and low destructive effect on adsorbent structure (Vakili et al., 2019). Thus, applying a proper agent with good characteristics will ensure a best regeneration of used adsorbents. Different agents such as alkalis, acids, chelating agents, salts, organic solvents and mixtures used for regenerating of chitosan/chitin-based composites loaded with various pollutants are summarized in Table 5.

The basic eluents such as NaOH can present better regeneration performance than other eluents. This can be explained by the greater tendency of pollutants toward Na^+ of alkali than active sites of the adsorbent and lower bonding between the adsorbent and adsorbate in alkaline medium. In this regard, Subedi et al. (2019) demonstrated that 0.1 M NaOH exhibited better regeneration performance than 0.1 M of HNO_3 for magnetic chitosan based adsorbent loaded with Cr(VI). After four successive adsorption-desorption cycles, the performance was reduced from 77.5 to 75% when NaOH eluent was used with a decrease from 70 to 32.5% using HNO_3. This finding could be related to high Cr (VI) adsorption at high acidic sample with pH of 2. Zhang et al. (2014) also demonstrated that the regeneration performance of different eluents towards magnetic chitosan-GO composite loaded with Hg(II) followed the order: NaOH < HNO_3 < EDTA < $Ca(NO_3)_2$. Chitosan-carbonaceous materials composite regenerated by NaOH exhibited the highest recycling times with slightly decrease in adsorption efficiency (Table 5). For example, magnetic chitosan-CNTs loaded with Cr(VI) showed a little reduction in adsorption performance of 5% after ten cycles (Neto et al., 2019). Also, magnetic chitosan-GO composite underwent 4% reduction in its adsorption capacity for Cr(VI) after 7 cycles (Zhang, Luo et al., 2016). The best regeneration by NaOH was also reported for the chitosan-CNTs composite/tri-nitro phenol (Khakpour & Tahermansouri, 2018) and chitosan-BC composite/ ciprofloxacin systems (Afzal et al., 2018). The desorption mechanism by basic eluents includes deprotonation and enrichment of negatively charged active sites in adsorbents. These steps weaken the electrostatic bonding between chitosan active groups and adsorbate ions and subsequent the separation of adsorbed ions from active sites (Kumar & Jiang, 2016). The basic reaction for the regeneration method by NaOH is given as follows:

$$\text{Chitosan-}NH_3^+\ Me^- + NaOH \rightarrow \text{Chitosan-}NH_2 + Me^-\ Na^+ + H_2O \quad (1)$$

HNO_3 and HCl are the most applied acidic eluents for desorption of pollutants from chitosan-carbonaceous material composites. These eluents are preferred for desorption of cationic species because of the favorable repulsion between protonated –NH_2 groups of composite and cationic species under acidic conditions. The presence of more H^+ ions in HCl solution can reduce the attraction of pollutants towards active groups and pollutant. Moreover, Cl^- ions are able to make a complex with cationic species and then liberate from the adsorbent (Vakili et al., 2019). HCl has been utilized for desorption of Cd(II) from magnetic chitosan-AC composite with 27 % reduction in adsorption capacity within 3 cycles (Sharififard et al., 2018). Also, the acid has used for desorbing Pb(II) from magnetic chitosan-GO composite with 14 % reduction in adsorption percentage within 4 cycles (Samuel et al., 2018). HNO_3 has also been performed by many researchers for desorption of pollutants adsorbed onto chitosan-carbonaceous materials composite adsorbents. In this regard, H^+ can displace by attracted ions on the adsorbent surface. Li et al. (2015) found an efficient regeneration method for chitosan-GO composite using 0.01 M HNO_3 with 3.8 %, 5.4 % and 7.4 % reduction in uptakes of Cd(II), Pb(II) and Cu(II) ions, respectively, within 3 cycles (Table 5). HNO_3 eluent of 1 M concentration was utilized for desorption of Cd(II) from magnetic chitosan-AC composite with 6% reduction in adsorption within 3 cycles (Yadaei et al., 2018). Thus, HNO_3 was highly active than HCl in elution of metals from chitosan-carbonaceous material composites. Li et al. (2015) also showed the preferable use of HNO_3 eluent for Cu(II), Cd(II), and Pb(II) ions from chitosan-GO composite with recovery percentages within (89–97 %) relative to (84–88 %) by using EDTA. The desorption mechanism by acidic eluents involved the protonation of adsorbent sites and the cationic exchange between H^+ and the adsorbates. This released the adsorbed ions into the eluent solution and reduced the adsorbed ions that interact with adsorbents (Vakili et al., 2019). This mechanism can be represented by the following reaction:

$$\text{Chitosan-}NH_2\ Me + H^+ \rightarrow \text{Chitosan-}NH_3^+ + Me \quad (2)$$

Several researches have addressed the regeneration performances of ethylene diamine tetra acetic acid (EDTA) and EDTA-disodium (Na_2EDTA) chelating agents for chitosan-carbonaceous material composites. EDTA molecule structure consists of N atoms and –COOH groups and commonly marketed as sodium salts. These agents have large tendency to make EDTA-metal complex and can displace the structural groups on the adsorbents (Vakili et al., 2019). EDTA eluent at concentration of 0.01 M exhibited better regeneration for chitosan-G composite loaded by Cd(II) ions with only 6% reduction in adsorption performance within 3 cycles (Mallakpour & Khadem, 2019). EDTA also desorbed Pb(II) from chitosan-CNTs composite with a decline of 13% in adsorption performance within 6 cycles (Wang et al., 2020). For Na_2-EDTA eluent only 5% decrease was reported in performance of chitosan-BC composite/Pb(II) (Zhang, Tang et al., 2019) and magnetic chitosan-AC composite/Cu(II) (Li et al., 2017) systems, respectively, within 4 and 5 cycles. Na_2-EDTA was also efficient in desorbing of rhodamine dye from magnetic chitosan-GO composite with only 6.8% decline in adsorption performance within 7 cycles (Marnani & Shahbazi, 2019).

Methanol, ethanol and acetone were also utilized for regeneration of chitosan-carbonaceous materials composite loaded with various pollutants. Methanol eluent was utilized to desorb ciprofloxacin from magnetic chitosan-GO composite with 22% decrease in adsorption performance after 4 cycles (Wang, Yang et al., 2016). Ethanol desorbed methylene blue dye from chitosan-GO composite with adsorption reduction of 35% within 5 cycles (Fan, Luo, Sun, Qiu, & Li, 2013). An efficient regeneration was obtained with acetone for magnetic chitosan-GO composite loaded with methyl violet and alizarin yellow R dyes with a drop in adsorption of 5 and 11%, respectively (Gul et al., 2016).

Sodium chloride (NaCl) agent depends on its ionic species (Na^+ and Cl^-. Na^+) can interact with the pollutants to form a complex and liberate from the adsorbent. The chloride ion can displace with the pollutants and contact with active sites on chitosan-carbonaceous materials composite adsorbents (Vakili et al., 2019). Banu et al. (2019) utilized 0.1 M NaCl eluent for regeneration of chitosan-AC composite loaded with nitrate and phosphate and reported a reduction of 47% and 16.5% in adsorption capacities of nitrate and phosphate after five cycles, respectively. Moreover, NaCl was also utilized for desorption of antibiotics including ciprofloxacin, erythromycin, and amoxicillin from magnetic chitosan-AC composite with desorption efficiency of 6, 10, and 100%, respectively within 3 h desorption time (Danalıoğlu et al., 2017). Using the same adsorption systems, NaCl showed better desorption performance with erythromycin and amoxicillin as compared to ethanol eluent. Meanwhile, for desorption of ciprofloxacin, ethanol eluent was the better than NaCl.

A combination of different eluents was utilized for regeneration of chitosan-carbonaceous materials composite loaded with various species. MB dye–loaded chitosan-GO composite was regenerated by treatment with 1 M HCl and ethanol. The finding demonstrated of 19.9% reduction in uptake of MB on chitosan-GO after five cycles (Yan et al., 2019). Chitosan-GO composite loaded with metanil yellow dye showed sufficient reusability during successive regeneration with 30 mL of 0.1 M NaOH for 1.5 h followed by 0.1 M HCl for 0.25 h. By this treatment, only 11% reduction in adsorption performance was reported within 5 cycles. The role of NaOH agent in elution process depends on the replacement of anionic dye species by OH^- ion. Hence, the treatment with HCl agent enhanced the protonation of the chitosan-GO surface which then exhibited high attraction for metanil yellow dye. A small decline in composite performance might be due to the partial deterioration of internal structure of chitosan-GO. In addition, chitosan-GO displayed loss some weight during the regeneration test (Lai, Hiew et al., 2019). A mixture of ethanol and acetic acid (0.5% acid) was effective when used as eluent for the regeneration of magnetic chitosan-G composite loaded with MB dye. The adsorption efficiency remained within the range between 99 – 97% even after five cycles. This suggested that the adsorbent could attract cationic dyes and showed reusability with more efficient separation (Hoa, Khong, Quyen, & Trung, 2016). Desorption of the linuron, isoproturon and monuron herbicides from magnetic chitosan-GO composite was carried out using methanol alone and a combination of 10 mL of chloroform and methanol (1:1) as eluents. The result of the recovery indicated high rate of recovery (92%, 90% and 94%) for these herbicides eluted with the mixture as compared to (84%, 76% and 85%) with the methanol alone, respectively (Shah et al., 2018).

According to the collected data (Table 5), the most frequently used agents to regenerate chitosan/chitin-carbonaceous material composites follow the order: alkalis < acids < chelating agents < organic solvents < mixtures. Alkali eluents such as NaOH can present better regeneration performance than other eluents in terms of the lowest reduction in adsorption performance within the highest recycling times. The combination of two eluents can enhance the regeneration performance relative to the use of individual eluent.

6. Conclusions and future perspectives

The preparation and adsorption application of chitosan/chitin-carbonaceous material composites were reviewed. From the published studies, the most widely used carbonaceous materials for preparation of chitosan/chitin-based composite were graphene oxide and activated carbon followed by carbon nanotubes, biochar and graphene. Activated carbon and graphene oxide exhibit biopolymer composites with the highest surface areas relative to other carbonaceous materials. The most treated pollutants were copper, chromium, cadmium and lead metals along with methylene blue dye. Other extensively studied pollutants were ciprofloxacin and tetracycline antibiotics and phenols. Chitosan/chitin-carbonaceous materials composite showed high uptake for pollutants relative to chitosan/chitin alone. Chitosan/chitin-GO and chitosan/chitin-AC composites showed high adsorption capacities towards most of pollutants relative to other composites. Chitosan composite adsorbent was more efficient as compared to chitin composite. Moreover, the incorporation of magnetic materials into composites enhanced the adsorption performance towards pollutants by development of composites structure. Most of studies included chitosan composites with few studies about chitin composites. Langmuir model well correlated the isotherm data of most pollutants on chitosan/chitin-carbonaceous material composites. Freundlich model with or without Langmuir model was also applicable in some cases. From the parameters of both models the adsorption process was favorable. PSO kinetic model showed best representation for kinetics data. Alkali eluents such as NaOH could present better regeneration performance than other eluents in terms of the lowest reduction in adsorption performance and the highest recycling times. The combination of two eluents could enhance the regeneration performance relative to the use of individual eluent. The analysis of adsorption factors showed that initial adsorbate concentration and adsorbent dosage exhibited significant effect on the adsorption of the studied pollutants relative to initial solution pH. The kinetics analysis confirmed that both the pore and film diffusion steps could determine the adsorption mechanism.

Chitosan/chitin-carbonaceous material composites can be promising adsorbents in the field of wastewater treatment due to their enhanced pore characteristics and high adsorption performances towards aquatic pollutants. Therefore, these adsorbents have been addressed in several studies. However, other works are still required such as (1) carrying out more studies on chitin-derived composites, (2) testing the use of other carbonaceous composite materials like carbon fiber, graphite, hydrochar or anthracite, (3) adopting more than one carbonaceous material to be combined with raw chitosan/chitin, (4) studying the influence of other parameters such as adsorbent particle size and shaking speed on adsorption process, (5) focusing on the selectivity of a specific adsorbent towards mixed pollutants, (6) investigation the application of chitosan/chitin derived adsorbents for the treatment of real wastewaters using fixed-bed adsorption system, and (7) utilization of these adsorbents for other applications as the removal of aquatic pollutants such as surfactants, fluorides, sulfur compounds, oils, aromatics, etc.

Acknowledgment

The publication of this article was funded by the Qatar National Library.

Appendix A. Supplementary data

Supplementary material related to this article can be found, in the online version, at doi:https://doi.org/10.1016/j.carbpol.2020.116690.

References

Abbasi, M., & Habibi, M. M. (2016). Optimization and characterization of direct blue 71 removal using nanocomposite of chitosan-MWCNTs: Central composite design modeling. *Journal of the Taiwan Institute of Chemical Engineers, 62*, 112–121.

Abd Malek, N. N., Jawad, A. H., Abdulhameed, A. S., Ismail, K., & Hameed, B. H. (2020). New magnetic Schiff's base-chitosan-glyoxal/fly ash/Fe_3O_4 biocomposite for the removal of anionic azo dye: An optimized process. *International Journal of Biological Macromolecules, 1461*, 530–539.

Abdel Salam, M., El-Shishtawy, R. M., & Obaid, A. Y. (2014). Synthesis of magnetic multi-walled carbon nanotubes/magnetite/ chitin magnetic nanocomposite for the removal of rose Bengal from real and model solution. *Journal of Industrial and Engineering Chemistry, 20*, 3559–3567.

Afzal, M. Z., Sun, X.-F., Liu, J., Song, C., Wang, S.-G., & Javed, A. (2018). Enhancement of ciprofloxacin sorption on chitosan/biochar hydrogel beads. *The Science of the Total Environment, 639*, 560–569.

Ahmad, M., Manzoor, K., & Ikram, S. (2017). Versatile nature of hetero-chitosan based derivatives as biodegradable adsorbent for heavy metal ions; a review. *International Journal of Biological Macromolecules, 105*, 190–203.

Ahmed, M. J. (2017). Adsorption of non-steroidal anti-inflammatory drugs from aqueous solution using activated carbons: Review. *Journal of Environmental Management, 190*, 274–282.

Ahmed, M. J., & Hameed, B. H. (2018). Removal of emerging pharmaceutical contaminants by adsorption in a fixed bed column: A review. *Ecotoxicology and Environmental Safety, 149*, 257–266.

Ahmed, M. J., & Hameed, B. H. (2019). Insights into the isotherm and kinetic models for the coadsorption of pharmaceuticals in the absence and presence of metal ions: A review. *Journal of Environmental Management, 252*, Article 109617.

Alves, D. C. S., Gonçalves, J. O., Coseglio, B. B., Burgo, T. A. L., Dotto, G. L., Pinto, L. A. A., et al. (2019). Adsorption of phenol onto chitosan hydrogel scaffold modified with carbon nanotubes. *Journal of Environmental Chemical Engineering, 7*, Article 103460.

Anush, S. M., Chandan, H. R., & Vishalakshi, B. (2019). Synthesis and metal ion adsorption characteristics of graphene oxide incorporated chitosan Schiff base. *International Journal of Biological Macromolecules, 126*, 908–916.

Arumugam, T. K., Krishnamoorthy, P., Rajagopalan, N. R., Nanthini, S., & Vasudevan, D. (2019). Removal of malachite green from aqueous solutions using a modified chitosan composite. *International Journal of Biological Macromolecules, 128*, 655–664.

Auta, M., & Hameed, B. H. (2013). Coalesced chitosan activated carbon composite for batch and fixed-bed adsorption of cationic and anionic dyes. *Colloids and Surfaces B,*

Biointerfaces, 105, 199–206.
Auta, M., & Hameed, B. H. (2014). Chitosan–clay composite as highly effective and low-cost adsorbent for batch and fixed-bed adsorption of methylene blue. *Chemical Engineering Journal, 2371*, 352–361.
Baig, N., Ihsanullah, S. M., & Saleh, T. A. (2019). Graphene-based adsorbents for the removal of toxic organic pollutants: A review. *Journal of Environmental Management, 244*, 370–382.
Bakshi, P. S., Selvakumar, D., Kadirvelu, K., & Kumar, N. S. (2020). Chitosan as an environment friendly biomaterial – A review on recent modifications and applications. *International Journal of Biological Macromolecules, 150*, 1072–1083.
Banerjee, P., Barman, S. R., Mukhopadhayay, A., & Das, P. (2017). Ultrasound assisted mixed azo dye adsorption by chitosan–graphene oxide nanocomposite. *Chemical Engineering Research and Design, 117*, 43–56.
Banu, H. T., Karthikeyan, P., & Meenakshi, S. (2019). Zr^{4+} ions embedded chitosan-soya bean husk activated bio-char composite beads for the recovery of nitrate and phosphate ions from aqueous solution. *International Journal of Biological Macromolecules, 130*, 573–583.
Bhatnagar, A., & Sillanpää, M. (2009). Applications of chitin- and chitosan-derivatives for the detoxification of water and wastewater – A short review. *Advances in Colloid and Interface Science, 152*, 26–38.
Chatterjee, S., Lee, M. W., & Woo, S. H. (2010). Adsorption of congo red by chitosan hydrogel beads impregnated with carbon nanotubes. *Bioresource Technology, 101*, 1800–1806.
Cui, X., Li, H., Yao, Z., Shen, Y., He, Z., Yang, X., et al. (2019). Removal of nitrate and phosphate by chitosan composited beads derived from crude oil refinery waste: Sorption and cost-benefit analysis. *Journal of Cleaner Production, 207*, 846–856.
Danalıoğlu, S. T., Bayazit, Ş. S., Kuyumcu, Ö. K., & Abdel Salam, M. (2017). Efficient removal of antibiotics by a novel magnetic adsorbent: Magnetic activated carbon/chitosan (MACC) nanocomposite. *Journal of Molecular Liquids, 240*, 589–596.
Dandil, S., Sahbaz, D. A., & Acikgoz, C. (2019). Adsorption of Cu(II) ions onto crosslinked chitosan/waste active sludge char (WASC) beads: Kinetic, equilibrium, and thermodynamic study. *International Journal of Biological Macromolecules, 136*, 668–675.
Daud, M., Hai, A., Banat, F., Wazir, M. B., Habib, M., Bharath, G., et al. (2019). A review on the recent advances, challenges and future aspect of layered double hydroxides (LDH) – Containing hybrids as promising adsorbents for dyes removal. *Journal of Molecular Liquids, 288*, Article 110989.
Debnath, S., Parashar, K., & Pillay, K. (2017). Ultrasound assisted adsorptive removal of hazardous dye Safranin O from aqueous solution using crosslinked graphene oxide-chitosan(GO CH) composite and optimization by response surface methodology (RSM) approach. *Carbohydrate Polymers, 175*, 509–517.
Dou, J., Gan, D., Huang, Q., Liu, M., Chen, J., Deng, F., et al. (2019). Functionalization of carbon nanotubes with chitosan based on MALI multicomponent reaction for Cu^{2+} removal. *International Journal of Biological Macromolecules, 136*, 476–485.
El Knidri, H., Belaabed, R., Addaou, A., Laajeb, A., & Lahsini, A. (2018). Extraction, chemical modification and characterization of chitin and chitosan. *International Journal of Biological Macromolecules, 120*, 1181–1189.
Fan, L., Luo, C., Sun, M., Li, X., & Qiu, H. (2013). Highly selective adsorption of lead ions by water-dispersible magnetic chitosan/graphene oxide composites. *Colloids and Surfaces B, Biointerfaces, 103*, 523–529.
Fan, L., Luo, C., Sun, M., Qiu, H., & Li, X. (2013). Synthesis of magnetic -cyclodextrin–chitosan/graphene oxide as nanoadsorbent and its application in dye adsorption and removal. *Colloids and Surfaces B, Biointerfaces, 103*, 601–607.
Fiyadh, S. S., AlSaadi, M. A., Jaafar, W. Z., AlOmar, M. K., Fayaed, S. S., Mohd, N. S., et al. (2019). Review on heavy metal adsorption processes by carbon nanotubes. *Journal of Cleaner Production, 230*, 783–793.
Foo, K. Y., & Hameed, B. H. (2012). Potential of jackfruit peel as precursor for activated carbon prepared by microwave induced NaOH activation. *Bioresource Technology, 112*, 143–150.
Foo, K. Y., & Hameed, B. H. (2011). Preparation of activated carbon from date stones by microwave induced chemical activation: Application for methylene blue adsorption. *Chemical Engineering Journal, 170*, 338–341.
Frindy, S., Primo, A., Ennajih, H., Qaiss, A., Bouhfid, R., Lahcini, M., et al. (2017). Chitosan–Graphene oxide films and CO_2-dried porous aerogel microspheres: Interfacial interplay and stability. *Carbohydrate Polymers, 167*, 297–305.
Garba, Z. N., Zhou, W., Lawan, I., Xiao, W., Zhang, M., Wang, L., et al. (2019). An overview of chlorophenols as contaminants and their removal from wastewater by adsorption: A review. *Journal of Environmental Management, 241*, 59–75.
Ghourbanpour, J., Sabzi, M., & Shafagh, N. (2019). Effective dye adsorption behavior of poly(vinyl alcohol)/chitin nanofiber/Fe(III) complex. *International Journal of Biological Macromolecules, 137*, 296–306.
González, J. A., Villanueva, M. E., Piehl, L. L., & Copello, G. J. (2015). Development of a chitin/graphene oxide hybrid composite for the removal of pollutant dyes: Adsorption and desorption study. *Chemical Engineering Journal, 280*, 41–48.
González, J. A., Bafico, J. G., Villanueva, M. E., Giorgieri, S. A., & Copello, G. J. (2018). Continuous flow adsorption of ciprofloxacin by using a nanostructured chitin/graphene oxide hybrid material. *Carbohydrate Polymers, 188*, 213–220.
Gul, K., Sohni, S., Waqar, M., Ahmad, F., Nik Norulaini, N. A., & Mohd. Omar, A. K. (2016). Functionalization of magnetic chitosan with graphene oxide for removal of cationic and anionic dyes from aqueous solution. *Carbohydrate Polymers, 152*, 520–531.
Guo, M., Wang, J., Wang, C., Strong, P. J., Jiang, P., Ok, Y. S., et al. (2019). Carbon nanotube-grafted chitosan and its adsorption capacity for phenol in aqueous solution. *The Science of the Total Environment, 682*, 340–347.
Hamed, I., Özogul, F., & Regenstein, J. M. (2016). Industrial applications of crustacean by-products (chitin, chitosan, and chitooligosaccharides): A review. *Trends in Food Science & Technology, 48*, 40–50.
Han, H., Rafiq, M. K., Zhou, T., Xu, R., Mašek, O., & Li, X. (2019). A critical review of clay-based composites with enhanced adsorption performance for metal and organic pollutants. *Journal of Hazardous Materials, 369*, 780–796.
Hasan, M., Ahmad, A. L., & Hameed, B. H. (2008). Adsorption of reactive dye onto cross-linked chitosan/oil palm ash composite beads. *Chemical Engineering Journal, 136*, 164–172.
Hejazi, F., Ghoreyshi, A. A., & Rahimnejad, M. (2019). Simultaneous phenol removal and electricity generation using a hybrid granular activated carbon adsorption-biodegradation process in a batch recycled tubular microbial fuel cell. *Biomass & Bioenergy, 129*, Article 105336.
Hoa, N. V., Khong, T. T., Quyen, T. T. H., & Trung, T. S. (2016). One-step facile synthesis of mesoporous graphene/Fe_3O_4/chitosan nanocomposite and its adsorption capacity for a textile dye. *Journal of Water Process Engineering, 9*, 170–178.
Hu, Q., Wang, Q., Feng, C., Zhang, Z., Lei, Z., & Shimizu, K. (2018). Insights into mathematical characteristics of adsorption models and physical meaning of corresponding parameters. *Journal of Molecular Liquids, 254*, 20–25.
Hu, D., Huang, H., Jiang, R., Wang, N., Xu, H., Wang, Y.-G., et al. (2019). Adsorption of diclofenac sodium on bilayer amino-functionalized cellulose nanocrystals/chitosan composite. *Journal of Hazardous Materials, 369*, 483–493.
Huang, B., Liu, Y., Li, B., Liu, S., Zeng, G., Zeng, Z., et al. (2017). Effect of Cu(II) ions on the enhancement of tetracycline adsorption by Fe_3O_4@SiO_2-Chitosan/graphene oxide nanocomposite. *Carbohydrate Polymers, 157*, 576–585.
Huang, Y., Lee, X., Macazo, F. C., Grattieri, M., Cai, R., & Minteer, S. D. (2018). Fast and efficient removal of chromium (VI) anionic species by a reusable chitosan-modified multi-walled carbon nanotube composite. *Chemical Engineering Journal, 339*, 259–267.
Hydari, S., Sharififard, H., Nabavinia, M., & Parvizi, M. R. (2012). A comparative investigation on removal performances of commercial activated carbon, chitosan biosorbent and chitosan/activated carbon composite for cadmium. *Chemical Engineering Journal, 193–194*, 276–282.
Iijima, S. (1991). Helical microtubules of graphitic carbon. *Nature, 354*, 56–58.
Islam, M. A., Tan, I. A. W., Benhouria, A., Asif, M., & Hameed, B. H. (2015). Mesoporous and adsorptive properties of palm date seed activated carbon prepared via sequential hydrothermal carbonization and sodium hydroxide activation. *Chemical Engineering Journal, 270*, 187–195.
Islam, M. A., Tan, Y. L., Islam, M. A., Romić, M., & Hameed, B. H. (2018). Chitosan–Bleaching earth clay composite as an efficient adsorbent for carbon dioxide adsorption: Process optimization. *Colloids and Surfaces A, Physicochemical and Engineering Aspects, 5545*, 9–15.
Islam, M. A., Ahmed, M. J., Khanday, W. A., Asif, M., & Hameed, B. H. (2017a). Mesoporous activated coconut shell-derived hydrochar prepared via hydrothermal carbonization-NaOH activation for methylene blue adsorption. *Journal of Environmental Management, 203*, 237–244.
Islam, M. A., Ahmed, M. J., Khanday, W. A., Asif, M., & Hameed, B. H. (2017b). Mesoporous activated carbon prepared from NaOH activation of rattan (Lacosperma secundiflorum) hydrochar for methylene blue removal. *Ecotoxicology and Environmental Safety, 138*, 279–285.
Jawad, A. H., Norrahma, S. S. A., Hameed, B. H., & Ismail, K. (2019). Chitosan-glyoxal film as a superior adsorbent for two structurally different reactive and acid dyes: Adsorption and mechanism study. *International Journal of Biological Macromolecules, 135*, 569–581.
Jiang, Y., Gong, J.-L., Zeng, G.-M., Ou, X.-M., Chang, Y.-N., Deng, C.-H., et al. (2016). Magnetic chitosan–graphene oxide composite for anti-microbial and dye removal applications. *International Journal of Biological Macromolecules, 82*, 702–710.
Karaer, H., & Kaya, I. (2016). Synthesis, characterization of magnetic chitosan/active charcoal composite and using at the adsorption of methylene blue and reactive blue 4. *Microporous and Mesoporous Materials, 232*, 26–38.
Karthikeyan, P., & Meenakshi, S. (2019). Synthesis and characterization of Zn–Al LDHs/activated carbon composite and its adsorption properties for phosphate and nitrate ions in aqueous medium. *Journal of Molecular Liquids, 296*, Article 111766.
Khakpour, R., & Tahermansouri, H. (2018). Synthesis, characterization and study of sorption parameters of multi-walled carbon nanotubes/chitosan nanocomposite for the removal of picric acid from aqueous solutions. *International Journal of Biological Macromolecules, 109*, 598–610.
Khanday, W. A., Asif, M., & Hameed, B. H. (2017). Cross-linked beads of activated oil palm ash zeolite/chitosan composite as a bio-adsorbent for the removal of methylene blue and acid blue 29 dyes. *International Journal of Biological Macromolecules, 95*, 895–902.
Khanday, W. A., Ahmed, M. J., Okoye, P. U., Hummadi, E. H., & Hameed, B. H. (2019). Single-step pyrolysis of phosphoric acid-activated chitin for efficient adsorption of cephalexin antibiotic. *Bioresource Technology, 280*, 255–259.
Kumar, A. S. K., & Jiang, S.-J. (2016). Chitosan-functionalized graphene oxide: A novel adsorbent an efficient adsorption of arsenic from aqueous solution. *Journal of Environmental Chemical Engineering, 4*, 1698–1713.
Kumari, H. J., Krishnamoorthy, P., Arumugam, T. K., Radhakrishnan, S., & Vasudevan, D. (2017). An efficient removal of crystal violet dye from waste water by adsorption onto TLAC/Chitosan composite: A novel low cost adsorbent. *International Journal of Biological Macromolecules, 96*, 324–333.
Lai, K. C., Hiew, B. Y. Z., Lee, L. Y., Gan, S., Thangalazhy-Gopakumara, S., Chiu, W. S., et al. (2019). Ice-templated graphene oxide/chitosan aerogel as an effective adsorbent for sequestration of metanil yellow dye. *Bioresource Technology, 274*, 134–144.
Lai, K. C., Lee, L. Y., Hiew, B. Y. Z., Thangalazhy-Gopakumar, S., & Gan, S. (2019). Environmental application of three-dimensional graphene materials as adsorbents for dyes and heavy metals: Review on ice-templating method and adsorption mechanisms. *Journal of Environmental Science, 79*, 174–199.

Lessa, E. F., Nunes, M. L., & Fajardo, A. R. (2018). Chitosan/waste coffee-grounds composite: An efficient and eco-friendly adsorbent for removal of pharmaceutical contaminants from water. *Carbohydrate Polymers, 189*, 257–266.
Li, Y., Sun, J., Du, Q., Zhang, L., Yang, X., Wu, S., et al. (2014). Mechanical and dye adsorption properties of graphene oxide/chitosan composite fibers prepared by wet spinning. *Carbohydrate Polymers, 102*, 755–761.
Li, X., Zhou, H., Wu, W., Wei, S., Xu, Y., & Kuang, Y. (2015). Studies of heavy metal ion adsorption on Chitosan/Sulfydrylfunctionalized graphene oxide composites. *Journal of Colloid and Interface Science, 448*, 389–397.
Li, A., Lin, R., Lin, C., He, B., Zheng, T., Lu, L., et al. (2016). An environment-friendly and multi-functional absorbent from chitosan for organic pollutants and heavy metal ion. *Carbohydrate Polymers, 148*, 272–280.
Li, J., Jiang, B., Liu, Y., Qiu, C., Hu, J., Qian, G., et al. (2017). Preparation and adsorption properties of magnetic chitosan composite adsorbent for Cu^{2+} removal. *Journal of Cleaner Production, 158*, 51–58.
Li, M.-F., Liu, Y.-G., Zeng, G.-M., Liu, N., & Liu, S.-B. (2019). Graphene and graphene-based nanocomposites used for antibiotics removal in water treatment: A review. *Chemosphere, 226*, 360–380.
Liu, L., Li, C., Bao, C., Jia, Q., Xiao, P., Liu, X., et al. (2012). Preparation and characterization of chitosan/graphene oxide composites for the adsorption of Au(III) and Pd(II). *Talanta, 93*, 350–357.
Liu, Y., Liu, R., Li, M., Yu, F., & He, C. (2019). Removal of pharmaceuticals by novel magnetic genipin-crosslinked chitosan/graphene oxide-SO_3H composite. *Carbohydrate Polymers, 220*, 141–148.
Liu, J., Zhou, B., Zhang, H., Ma, J., Mu, B., & Zhang, W. (2019). A novel biochar modified by chitosan-Fe/S for tetracycline adsorption and studies on site energy distribution. *Bioresource Technology, 294*, Article 122152.
Lu, F., Dong, A., Ding, G., Xu, K., Li, J., & You, L. (2019). Magnetic porous polymer composite for high performance adsorption of acid red 18 based on melamine resin and chitosan. *Journal of Molecular Liquids, 294*, Article 111515.
Luo, J., Fan, C., Xiao, Z., Sun, T., & Zhou, X. (2019). Novel graphene oxide/carboxymethyl chitosan aerogels via vacuum-assisted self-assembly for heavy metal adsorption capacity. *Colloids and Surfaces A, Physicochemical and Engineering Aspects, 578*, Article 123584.
Ma, Z., Liu, D., Zhu, Y., Li, Z., Li, Z., Tian, H., et al. (2016). Graphene oxide/chitin nanofibril composite foams as column adsorbents for aqueous pollutants. *Carbohydrate Polymers, 144*, 230–237.
Mallakpour, S., & Khadem, E. (2019). Linear and nonlinear behavior of crosslinked chitosan/N-doped graphene quantum dot nanocomposite films in cadmium cation uptake. *The Science of the Total Environment, 690*, 1245–1253.
Marnani, N. N., & Shahbazi, A. (2019). A novel environmental-friendly nanobiocomposite synthesis by EDTA and chitosan functionalized magnetic graphene oxide for high removal of Rhodamine B: Adsorption mechanism and separation property. *Chemosphere, 218*, 715–725.
Marrakchi, F., Khanday, W. A., Asif, M., & Hameed, B. H. (2016). Cross-linked chitosan/sepiolite composite for the adsorption of methylene blue and reactive orange 16. *International Journal of Biological Macromolecules, 93*, 1231–1239.
Marrakchi, F., Ahmed, M. J., Khanday, W. A., Asif, M., & Hameed, B. H. (2017). Mesoporous-activated carbon prepared from chitosan flakes via single-step sodium hydroxide activation for the adsorption of methylene blue. *International Journal of Biological Macromolecules, 98*, 233–239.
Masih, M., Anthony, P., & Siddiqui, S. H. (2018). Removal of Cu (II) ion from aqueous solutions by rice husk carbon-chitosan composite gel (CCRH) using response surface methodology. *Environmental Nanotechnology Monitoring & Management, 10*, 189–198.
Miretzky, P., & Cirelli, A. F. (2009). Hg(II) removal from water by chitosan and chitosan derivatives: A review. *Journal of Hazardous Materials, 167*, 10–23.
Miretzky, P., & Cirelli, A. F. (2011). Fluoride removal from water by chitosan derivatives and composites: A review. *Journal of Fluorine Chemistry, 132*, 231–240.
Mo, J., Yang, Q., Zhang, N., Zhang, W., Zheng, Y., & Zhien (2018). A review on agro-industrial waste (AIW) derived adsorbents for water and wastewater treatment. *Journal of Environmental Management, 227*, 395–405.
Muxika, A., Etxabide, A., Uranga, J., Guerrero, P., & de la Caba, K. (2017). Chitosan as a bioactive polymer: Processing, properties and applications. *International Journal of Biological Macromolecules, 105*, 1358–1368.
Neto, J. D. M., Bellato, C. R., & Silva, D. D. (2019). Iron oxide/carbon nanotubes/chitosan magnetic composite film for chromium species removal. *Chemosphere, 218*, 391–401.
Nitayaphat, W., & Jintakosol, T. (2015). Removal of silver(I) from aqueous solutions by chitosan/bamboo charcoal composite beads. *Journal of Cleaner Production, 87*, 850–855.
Olivera, S., Muralidhara, H. B., Venkatesh, K., Guna, V. K., Gopalakrishna, K., & Yogesh Kumar, K. (2016). Potential applications of cellulose and chitosan nanoparticles/composites in wastewater treatment: A review. *Carbohydrate Polymers, 153*, 600–618.
Omidi, S., & Kakanejadifard, A. (2018). Eco-friendly synthesis of graphene–chitosan composite hydrogel as efficient adsorbent for Congo red. *Royal Society of Chemistry Advances, 8*, 12179–12189.
Parlayıcı, Ş., & Pehlivan, E. (2019). Removal of chromium (VI) from aqueous solution using chitosan doped with carbon nanotubes. *Materials Today Proceedings, 18*, 1978–1985.
Peng, W., Li, H., Liu, Y., & Song, S. (2017). A review on heavy metal ions adsorption from water by graphene oxide and its composites. *Journal of Molecular Liquids, 230*, 496–504.
Rahmi, L., & Nurfatimah, R. (2018). Preparation of polyethylene glycol diglycidyl ether (PEDGE) crosslinked chitosan/activated carbon composite film for Cd^{2+} removal. *Carbohydrate Polymers, 199*, 499–505.
Reddy, D. H. K., & Lee, S.-M. (2013). Application of magnetic chitosan composites for the removal of toxic metal and dyes from aqueous solutions. *Advances in Colloid and Interface Science, 201–202*, 68–93.
Salzano de Luna, M., Ascione, C., Santillo, C., Verdolotti, L., Lavorgna, M., Buonocore, G. G., et al. (2019). Optimization of dye adsorption capacity and mechanical strength of chitosan aerogels through crosslinking strategy and graphene oxide addition. *Carbohydrate Polymers, 211*, 195–203.
Samuel, M. S., Shah, S. S., Bhattacharya, J., Subramaniam, K., & Pradeep Singh, N. D. (2018). Adsorption of Pb(II) from aqueous solution using a magnetic chitosan/graphene oxide composite and its toxicity studies. *International Journal of Biological Macromolecules, 115*, 1142–1150.
Samuel, M. S., Bhattacharya, J., Raj, S., Santhanam, N., Singh, H., & Pradeep Singh, N. D. (2019). Efficient removal of Chromium(VI) fromaqueous solution using chitosan grafted graphene oxide (CS-GO) nanocomposite. *International Journal of Biological Macromolecules, 121*, 285–292.
Sano, L. L., Krueger, A. M., & Landrum, P. F. (2005). Chronic toxicity of glutaraldehyde: Differential sensitivity of three freshwater organisms. *Aquatic Toxicology, 71*, 283–296.
Sarkar, B., Mandal, S., Tsang, Y. F., Kumar, P., Kim, K.-H., & Ok, Y. S. (2018). Designer carbon nanotubes for contaminant removal in water and wastewater: A critical review. *The Science of the Total Environment, 612*, 561–581.
Sarode, S., Upadhyay, P., Khosa, M. A., Mak, T., Shakir, A., Song, S., et al. (2019). Overview of wastewater treatment methods with special focus on biopolymer chitin-chitosan. *International Journal of Biological Macromolecules, 121*, 1086–1100.
Shah, J., Jan, M. R., & Tasmia (2018). Magnetic chitosan graphene oxide composite for solid phase extraction of phenylurea herbicides. *Carbohydrate Polymers, 199*, 461–472.
Shan, W., Zhang, D., Wang, X., Wang, D., Xing, Z., Xiong, Y., et al. (2019). One-pot synthesis of mesoporous chitosan-silica composite from sodium silicate for application in Rhenium (VII) adsorption. *Microporous and Mesoporous Materials, 278*, 44–53.
Sharififard, H., Shahraki, Z. H., Rezvanpanah, E., & Rad, S. H. (2018). A novel natural chitosan/activated carbon/iron bio-nanocomposite: Sonochemical synthesis, characterization, and application for cadmium removal in batch and continuous adsorption process. *Bioresource Technology, 270*, 562–569.
Sherlala, A. I. A., Raman, A. A. A., Bello, M. M., & Asghar, A. (2018). A review of the applications of organo-functionalized magnetic graphene oxide nanocomposites for heavy metal adsorption. *Chemosphere, 193*, 1004–1017.
Song, X., Huang, X., Li, Z., Li, Z., Wu, K., Jiao, Y., et al. (2019). Construction of blood compatible chitin/graphene oxide composite aerogel beads for the adsorption of bilirubin. *Carbohydrate Polymers, 207*, 704–712.
Soni, U., Bajpai, J., Singh, S. K., & Bajpai, A. K. (2017). Evaluation of chitosan-carbon based biocomposite for efficient removal of phenols from aqueous solutions. *Journal of Water Process Engineering, 16*, 56–63.
Subedi, N., Lähde, A., Abu-Danso, E., Iqbal, J., & Bhatnagar, A. (2019). A comparative study of magnetic chitosan (Chi@Fe_3O_4) and graphene oxide modified magnetic chitosan (Chi@Fe_3O_4GO) nanocomposites for efficient removal of Cr(VI) from water. *International Journal of Biological Macromolecules, 137*, 948–959.
Tran, V. S., Ngo, H. H., Guo, W., Zhang, J., Liang, S., Ton-That, C., et al. (2015). Typical low cost biosorbents for adsorptive removal of specific organic pollutants from water. *Bioresource Technology, 182*, 353–363.
Vakili, M., Rafatullah, M., Salamatinia, B., Abdullah, A. Z., Ibrahim, M. H., Tan, K. B., et al. (2014). Application of chitosan and its derivatives as adsorbents for dye removal from water and wastewater: A review. *Carbohydrate Polymers, 113*, 115–130.
Vakili, M., Deng, S., Cagnetta, G., Wang, W., Meng, P., Liu, D., et al. (2019). Regeneration of chitosan-based adsorbents used in heavy metal adsorption: A review. *Separation and Purification Technology, 224*, 373–387.
Vidal, R. R. L., & Moraes, J. S. (2019). Removal of organic pollutants from wastewater using chitosan: A literature review. *International Journal of Environmental Science and Technology, 16*, 1741–1754.
Wan Ngah, W. S., Teong, L. C., & M.A.K.M, H. (2011). Adsorption of dyes and heavy metal ions by chitosan composites: A review. *Carbohydrate Polymers, 83*, 1446–1456.
Wang, Y., Shi, L., Gao, L., Wei, Q., Cui, L., Hu, L., et al. (2015). The removal of lead ions from aqueous solution by using magnetic hydroxypropyl chitosan/oxidized multi-walled carbon nanotubes composites. *Journal of Colloid and Interface Science, 451*, 7–14.
Wang, Y., Guo, L., Qi, P., Liu, X., & Wei, G. (2019). Synthesis of three-dimensional graphene-based hybrid materials for water purification: A review. *Nanomaterials, 9*, 1123.
Wang, H., Shang, H., Sun, X., Hou, L., Wen, M., & Qiao, Y. (2020). Preparation of thermosensitive surface ion-imprinted polymers based on multi-walled carbon nanotube composites for selective adsorption of lead(II) ion. *Colloids and Surfaces A, Physicochemical and Engineering Aspects, 585*, Article 124139.
Wang, J., Wang, L., Yu, H., Zain-ul-Abdin, C. Y., Chen, Q., Zhou, W., et al. (2016). Recent progress on synthesis, property and application of modified chitosan: An overview. *International Journal of Biological Macromolecules, 88*, 333–344.
Wang, F., Yang, B., Wang, H., Song, Q., Tan, F., & Cao, Y. (2016). Removal of ciprofloxacin from aqueous solution by a magnetic chitosan grafted graphene oxide composite. *Journal of Molecular Liquids, 222*, 188–194.
Wong, S., Ngadi, N., Inuwa, I. M., & Hassan, O. (2018). Recent advances in applications of activated carbon from biowaste for wastewater treatment: A short review. *Journal of Cleaner Production, 175*, 361–375.
Wu, Y., Xia, C., Cai, L., & Shi, S. Q. (2018). Controlling pore size of activated carbon through self-activation process for removing contaminants of different molecular sizes. *Journal of Colloid and Interface Science, 518*, 41–47.
Wu, M., Zhao, S., Jing, R., Shao, Y., Liu, X., Lv, F., et al. (2019). Competitive adsorption of antibiotic tetracycline and ciprofloxacin on Montmorillonite. *Applied Clay Science, 180*, Article 105175.
Xiao, F., Cheng, J., Cao, W., Yang, C., Chen, J., & Luo, Z. (2019). Removal of heavy metals

from aqueous solution using chitosan-combined magnetic biochars. *Journal of Colloid and Interface Science, 540*, 579–584.
Yadaei, H., Beyki, M. H., Shemirani, F., & Nouroozi, S. (2018). Ferrofluid mediated chitosan@mesoporous carbon nanohybrid for green adsorption/preconcentration of toxic Cd(II): Modeling, kinetic and isotherm study. *Reactive & Functional Polymers, 122*, 85–97.
Yagub, M. T., Sen, T. K., Afroze, S., & Ang, H. M. (2014). Dye and its removal from aqueous solution by adsorption: A review. *Advances in Colloid and Interface Science, 209*, 172–184.
Yan, M., Huang, W., & Li, Z. (2019). Chitosan cross-linked graphene oxide/lignosulfonate composite aerogel for enhanced adsorption of methylene blue in water. *International Journal of Biological Macromolecules, 136*, 927–935.
Yu, B., Xu, J., Liu, J.-H., Yang, S.-T., Luo, J., Zhou, Q., et al. (2013). Adsorption behavior of copper ions on graphene oxide–chitosan aerogel. *Journal of Environmental Chemical Engineering, 1*, 1044–1050.
Zhang, Y., Yan, T., Yan, L., Guo, X., Cui, L., Wei, Q., et al. (2014). Preparation of novel cobalt ferrite/chitosan grafted with graphene composite as effective adsorbents for mercury ions. *Journal of Molecular Liquids, 198*, 381–387.
Zhang, C., Chen, Z., Guo, W., Zhu, C., & Zou, Y. (2018). Simple fabrication of chitosan/graphene nanoplates composite spheres for efficient adsorption of acid dyes from aqueous solution. *International Journal of Biological Macromolecules, 112*, 1048–1054.
Zhang, L., Luo, H., Liu, P., Fang, W., & Geng, J. (2016). A novel modified graphene oxide/chitosan composite used as an adsorbent for Cr(VI) in aqueous solutions. *International Journal of Biological Macromolecules, 87*, 586–596.
Zhang, L., Tang, S., He, F., Liu, Y., Mao, W., & Guan, Y. (2019). Highly efficient and selective capture of heavy metals by poly(acrylic acid) grafted chitosan and biochar composite for wastewater treatment. *Chemical Engineering Journal, 378*, Article 122215.
Zhang, L., Zeng, Y., & Cheng, Z. (2016). Removal of heavy metal ions using chitosan and modified chitosan: A review. *Journal of Molecular Liquids, 214*, 175–191.
Zhang, Z., Zhu, Z., Shen, B., & Liu, L. (2019). Insights into biochar and hydrochar production and applications: A review. *Energy, 171*, 581–598.
Zhu, H. Y., Jiang, R., Xiao, L., & Zeng, G. M. (2010). Preparation, characterization, adsorption kinetics and thermodynamics of novel magnetic chitosan enwrapping nanosized γ-Fe_2O_3 and multi-walled carbon nanotubes with enhanced adsorption properties for methyl orange. *Bioresource Technology, 101*, 5063–5069.